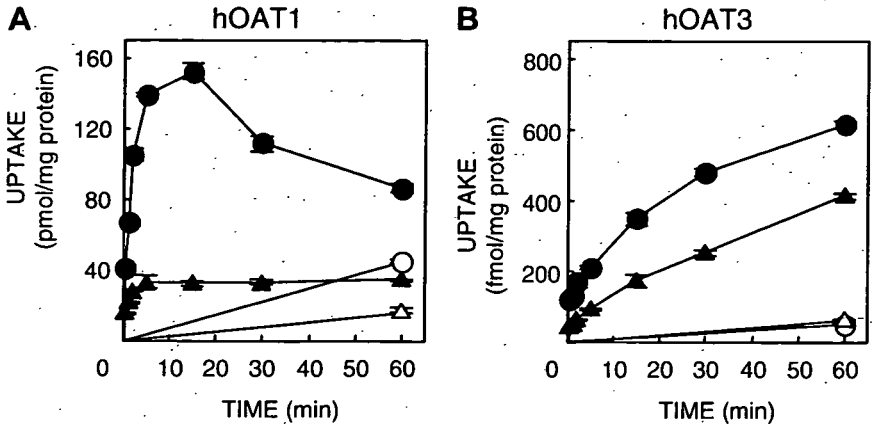

Fig. 2. Effects of extracellular Cl^- on the time course of the accumulation of *p*-[^{14}C]aminohippurate in HEK-hOAT1 (*A*) and [^{3}H]estrone sulfate in HEK-hOAT3 (*B*). *A*: HEK-pBK (△, ○) and HEK-hOAT1 (▲, ●) were incubated in Cl^--free (△, ▲) or Cl^--containing (●, ○) incubation medium with 5 μM *p*-[^{14}C]aminohippurate at 37°C for specified periods. *B*: HEK-pBK (△, ○) and HEK-hOAT3 (▲, ●) were incubated in Cl^--free (△, ▲) or Cl^--containing (○, ●) incubation medium with 10 nM [^{3}H]estrone sulfate at 37°C for specified periods. Each point represents the mean ± SE of 3 monolayers from a typical experiment.

was replaced with 1 ml of each incubation medium containing cefotiam. At the end of the incubation, the medium was aspirated, and then cells were washed three times with 2 ml of ice-cold incubation medium. To measure the accumulation of cefotiam, the cells were scraped and homogenized with 0.5 ml of distilled water. Protein levels were determined with 5 μl of the homogenate. For measuring the amount of cefotiam, 50 μl of distilled water and 10 μl of phosphoric acid were added to 0.45 ml of the homogenate, and the solution was mixed for 30 s. Then, 0.5 ml of the sample was loaded onto an Oasis HLB cartridge (Waters, Milford, MA) preconditioned with 1 ml each of methanol and distilled water. The column was washed with 1 ml of 5% methanol, and cefotiam was eluted from the column with 1 ml of methanol. The eluate was evaporated dry at 45–50°C and resuspended in 130 μl of distilled water. The solution was filtered through a 0.45-μm polyvinylidene fluoride filter. The concentration of cefotiam was measured using a high-performance liquid chromatograph (LC-10AT, LC-10AD; Shimadzu, Kyoto, Japan) equipped with a UV spectrophotometric detector (SPD-10AV, SPD-10A, Shimadzu) under the following conditions: column, Zorbax ODS column, 4.6-mm inside diameter × 250 mm (Du Pont, Wilmington, DE); mobile phase, 30 mM phosphate buffer (pH 6.5) in methanol at 78:22; flow rate, 0.8 ml/min; wave length, 254 nm; injection volume, 50 μl; temperature, 40°C.

Measurement of intracellular α-ketoglutarate. Intracellular α-ketoglutarate (α-KG) concentration was determined by the fluorimetric method of Williamson and Corkey (23). Briefly, HEK-pBK, HEK-hOAT1, and HEK-hOAT3 cells were seeded on poly-D-lysine-coated 35-mm dishes at a density of 1×10^6 cells/dish. At 48 h after seeding, the cells were used for the experiments. The cells were incubated with 0.5 ml of 3% $HClO_4$ for 30 min on ice to extract intracellular α-KG and to denature protein. After incubation, the buffer was transferred into a microtube and neutralized by 62 μl of 3 M NaOH. The amount of extracted α-KG in the neutralized buffer was measured by an enzymatic analysis. The conversions of α-KG and aspartate to glutamate and oxaloacetate, respectively, were catalyzed by aspartate aminotransferase. The oxaloacetate was then converted to malate by malate dehydrogenase. The associated conversion of NADH to NAD^+ was determined fluorimetrically (excitation, 355 nm; emission, 460 nm) at 37°C with MIthras LB940 (Berthold Technologies, Bad Wildbad, Germany).

Measurement of intracellular Cl^- concentration. Intracellular concentration of Cl^- was determined by the use of the Cl^--sensitive fluorophore SPQ (4, 11). HEK-pBK cells were seeded on a 96-well polystyrene plate at a density of 4×10^4 cells/well, and at 48 h after seeding, the cells were used for the experiments. The composition of *solution 1* was as follows (in mM): 106 NaCl, 24 Na gluconate, 5 K gluconate, 2 $CaCl_2$, 2 $MgCl_2$, 5 D-glucose, and 5 HEPES (pH 7.4). And the composition of KSCN medium was as follows (in mM): 145 KSCN, 1 $CaCl_2$, 0.5 $MgCl_2$, 5 D-glucose, and 5 HEPES (pH 7.4). According to a previous report (4), SPQ was loaded into the cells by incubation in a 1:1 mixture of *solution 1* and distilled water containing 5 mM SPQ at 23°C for 4 min. Then, the cells were washed two times with 0.2 ml of Cl^-(−) high-K medium and incubated with 0.1 ml of high-K medium containing each concentration of Cl^-, 5 μM nigericin, and 10 μM tributyltin at 37°C. During the incubation, SPQ fluorescence was measured (excitation, 355 nm; emission, 460 nm) with MIthras LB940. The background signal due to cell and instrument autofluorescence was obtained by incubation of the cells with 0.1 ml of KSCN medium containing 5 μM valinomycin, which has been shown to quench 99% of SPQ fluorescence (4). Data were fitted to the Stern-Volmer quenching equation: $F_0/F_{Cl} = 1 + K_q[Cl^-]$, where F_0 is the fluorescence in the absence of Cl^-, F_{Cl} is the fluorescence in the presence of each concentration of Cl^-, K_q is the Stern-Volmer constant, and $[Cl^-]$ is the concentration of Cl^-.

Statistical analysis. Data were analyzed statistically using a non-paired *t*-test. Multiple comparisons were performed using Scheffé's test. Probability values of <5% were considered significant.

RESULTS

Effects of extracellular anions on the uptake of p-[^{14}C]aminohippurate and [^{3}H]estrone sulfate by HEK-hOAT1 and HEK-hOAT3, respectively. The effects of extracellular anions on the transport of organic anions via hOAT1 and hOAT3 were examined, using *p*-[^{14}C]aminohippurate and [^{3}H]estrone sulfate, respectively, as model substrates. As shown in Fig. 1, the uptake

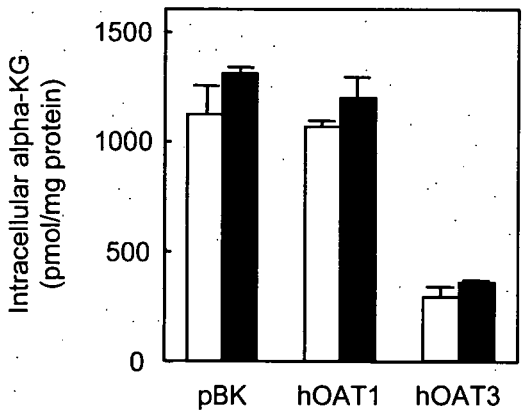

Fig. 3. Effect of extracellular Cl^- on the intracellular concentration of α-ketoglutarate (α-KG). After incubation in Cl^--free (open column) or Cl^--containing (black column) incubation medium at 37°C for 1 min, intracellular concentration of α-KG was determined. Each column represents the mean ± SE of 3 monolayers from a typical experiment.

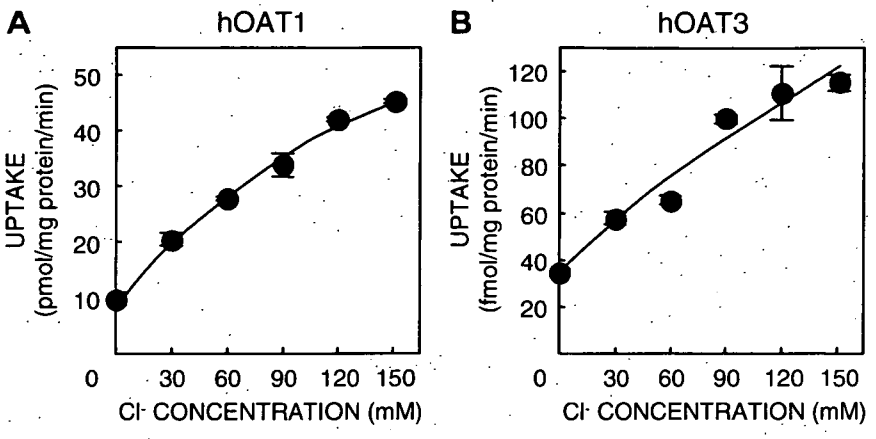

Fig. 4. Effects of extracellular Cl^- at various concentrations on the uptake of *p*-[^{14}C]aminohippurate by HEK-hOAT1 (*A*) and [^{3}H]estrone sulfate by HEK-hOAT3 (*B*). HEK-hOAT1 (*A*) and HEK-hOAT3 (*B*) were incubated with 5 μM *p*-[^{14}C]aminohippurate and 10 nM [^{3}H]estrone sulfate, respectively, in incubation medium containing various concentrations of Cl^- at 37°C for 1 min. The values were obtained by subtracting the values for the uptake in HEK-pBK from those in HEK-hOAT1 or HEK-hOAT3. The concentration of Cl^- was adjusted by replacing Cl^- with gluconate. Each point represents the mean ± SE of 3 monolayers from a typical experiment.

of *p*-[^{14}C]aminohippurate by HEK-hOAT1 with each anion was stimulated in the following order: $Cl^- > Br^- > SO_4^{2-} >$ gluconate. The rank order observed in the uptake of [^{3}H]estrone sulfate by HEK-hOAT3 was $Cl^- = Br^- > SO_4^{2-} >$ gluconate.

Effects of extracellular Cl^- on the uptake of various compounds by HEK-hOAT1 and HEK-hOAT3. In the subsequent experiments, the Cl^-(−) incubation medium, where Cl^- was substituted with gluconate, and the Cl^-(+) incubation medium were used. The uptake of *p*-[^{14}C]aminohippurate, [^{3}H]estrone sulfate, [^{3}H]cimetidine, [^{3}H]methotrexate, [^{14}C]captopril, [^{3}H]ochratoxin A, and cefotiam by HEK-hOAT1 and HEK-hOAT3 was evaluated in the absence or presence of extracellular Cl^-(Table 1). The uptake of *p*-[^{14}C]aminohippurate, [^{3}H]cimetidine, [^{3}H]methotrexate, [^{14}C]captopril, and [^{3}H]ochratoxin A by HEK-hOAT1 was significantly greater in the presence than absence of Cl^-. The uptake of *p*-[^{14}C]aminohippurate, [^{3}H]estrone sulfate, [^{3}H]cimetidine, [^{3}H]methotrexate, [^{3}H]ochratoxin A, and cefotiam by HEK-hOAT3 was significantly higher in the Cl^--containing medium than in Cl^--free medium. However, the uptake of [^{14}C]captopril by HEK-hOAT3 was not affected. The reason for this could be as follows: as shown in Table 1, the uptake of [^{14}C]captopril by HEK-pBK was significantly reduced when gluconate was replaced with Cl^-, indicating that the increase in the transporter-mediated uptake caused by Cl^- was masked.

Characterization of the effects of Cl^- on hOAT1 and hOAT3. Figure 2 shows the time course of uptake of *p*-[^{14}C]aminohippurate and [^{3}H]estrone sulfate by HEK-hOAT1 and HEK-

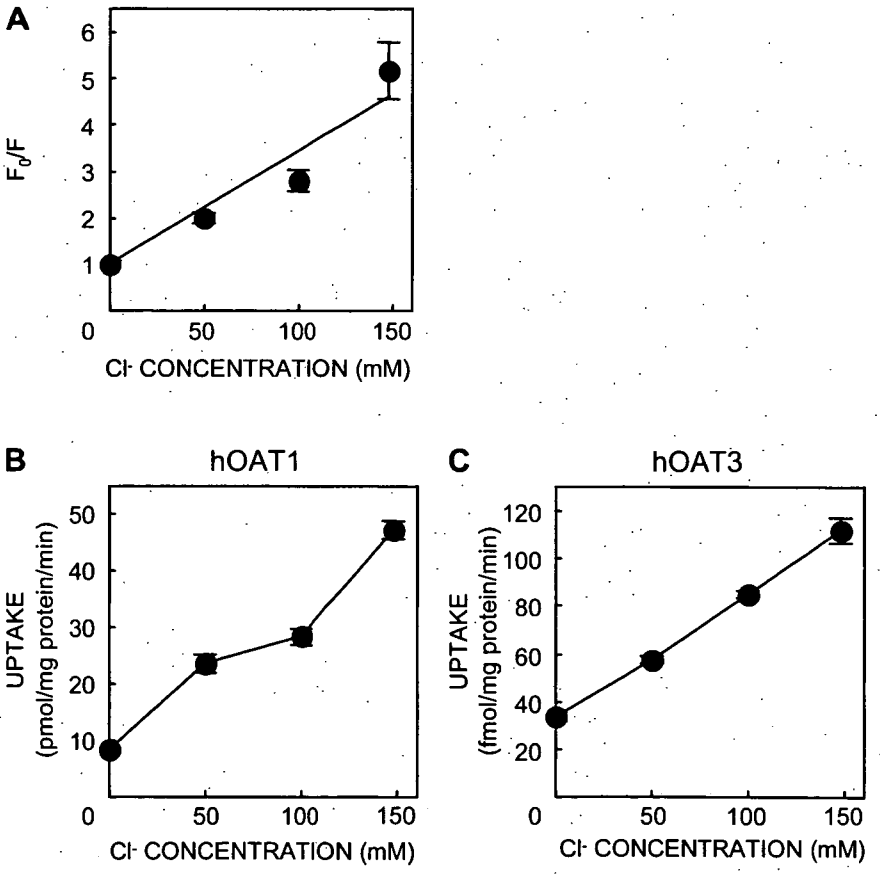

Fig. 5. *A*: the change of intracellular Cl^- concentration induced by high-K medium containing various concentrations of Cl^-, nigericin, and tributyltin. After loading with SPQ, HEK-pBK were incubated in high-K medium containing various concentrations of Cl^-, 5 μM nigericin, and 10 μM tributyltin at 37°C. During the incubation, SPQ fluorescence was measured. The change of fluorescence was fitted to the Stern-Volmer quenching equation (see MATERIALS AND METHODS for further details). The ordinate (F_0/F_{Cl}) is the total fluorescence measured in the absence of Cl^- divided by that measured in the presence of each concentration of Cl^-. *B* and *C*: effects of Cl^- at various concentrations on the uptake of *p*-[^{14}C]aminohippurate by HEK-hOAT1 and [^{3}H]estrone sulfate by HEK-hOAT3 under the conditions in which intracellular and extracellular Cl^- are equilibrated. HEK-hOAT1 (*B*) and HEK-hOAT3 (*C*) were incubated with 5 μM *p*-[^{14}C]aminohippurate and 10 nM [^{3}H]estrone sulfate, respectively, in high-K medium containing various concentrations of Cl^-, 5 μM nigericin, and 10 μM tributyltin at 37°C for 1 min. The values were obtained by subtracting the values for the uptake in HEK-pBK from those in HEK-hOAT1 or HEK-hOAT3. The concentration of Cl^- was adjusted by replacing Cl^- with gluconate. Each point represents the mean ± SE of 3 or 4 monolayers from a typical experiment.

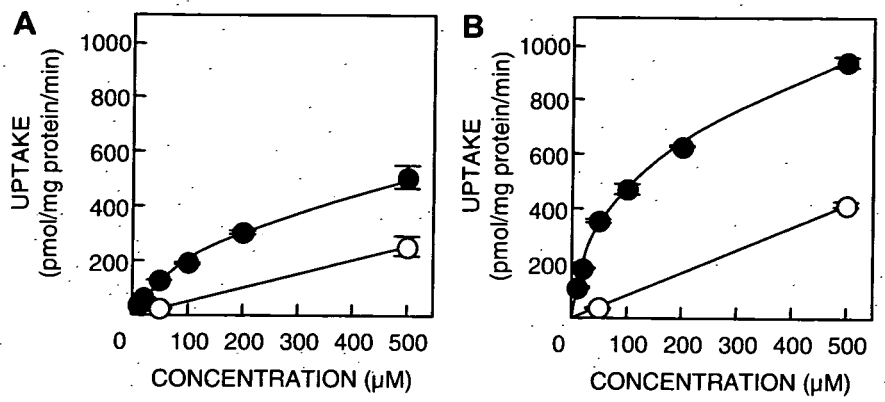

Fig. 6. Effect of extracellular Cl^- on the concentration-dependent uptake of *p*-[^{14}C]aminohippurate by HEK-hOAT1. HEK-hOAT1 were incubated in Cl^--free (*A*) or Cl^--containing (*B*) incubation medium with various concentrations of *p*-[^{14}C]aminohippurate in the absence (●) or presence (○) of unlabeled 5 mM *p*-aminohippurate at 37°C for 1 min. Each point represents the mean ± SE of 3 monolayers from a typical experiment.

hOAT3, respectively, in the absence or presence of extracellular Cl^-. The uptake of *p*-[^{14}C]aminohippurate and [^{3}H]estrone sulfate by HEK-hOAT1 and HEK-hOAT3, respectively, was greater in the Cl^-(+) incubation medium than the Cl^-(−) medium throughout.

OAT1 and OAT3 are organic anion/dicarboxylate exchangers (18, 19), and intracellular α-KG, endogenous dicarboxylate, is involved in the uptake of organic anions by HEK-hOAT1 and HEK-hOAT3. Therefore, we examined the effect of extracellular Cl^- on the intracellular concentration of α-KG. When HEK-pBK, HEK-hOAT1, and HEK-hOAT3 were incubated with Cl^-(+) incubation medium, the intracellular concentrations of α-KG were not changed compared with cells incubated with Cl^-(−) incubation medium (Fig. 3).

Next, the effects of extracellular Cl^- at various concentrations on the uptake of *p*-[^{14}C]aminohippurate and [^{3}H]estrone sulfate by HEK-hOAT1 and HEK-hOAT3, respectively, were examined. The concentration of extracellular Cl^- was adjusted by replacing Cl^- with gluconate. The uptake of *p*-[^{14}C]aminohippurate and [^{3}H]estrone sulfate by HEK-hOAT1 and HEK-hOAT3, respectively, was increased with the elevation in the concentration of extracellular Cl^- (Fig. 4).

Moreover, the effects of Cl^- at various concentrations on the uptake of *p*-[^{14}C]aminohippurate and [^{3}H]estrone sulfate by HEK-hOAT1 and HEK-hOAT3, respectively, were examined when there were no concentration gradients of Cl^- across plasma membranes. We adjusted the Cl^- concentration by substituting gluconate for it. The concentration of intracellular Cl^- was kept equal to that of extracellular Cl^- by using a high-K medium, the K^+/H^+ exchange ionophore nigericin, and the Cl^-/OH^- exchange ionophore tributyltin (4, 11). The high-K medium in the presence of nigericin clamps internal pH at the external pH and strongly depolarizes cell membrane potential. The addition of tributyltin to pH-clamped cells results in equal intracellular and extracellular Cl^- concentrations. At first, we confirmed the change of internal Cl^- concentration using the Cl^--sensitive fluorophore SPQ (4, 11). Chloride ion quenches the fluorescence of SPQ, and this compound is used to determine intracellular Cl^-. The change of fluorescence induced by medium containing each concentration of Cl^- was fitted to the Stern-Volmer quenching equation (Fig. 5*A*). There was a linear correlation between change in fluorescence and Cl^- concentration, indicating that intracellular concentration of Cl^- was changed in parallel with extracellular concentration. Figure 5, *B* and *C*, shows that the uptake of *p*-[^{14}C]aminohippurate and [^{3}H]estrone sulfate by HEK-hOAT1 and HEK-hOAT3, respectively, was increased in proportion to Cl^- concentration. Although we simultaneously measured the intracellular α-KG level in HEK-pBK at each Cl^- concentration, α-KG level was not affected by Cl^- concentration (data not shown).

Furthermore, the concentration-dependent uptake of *p*-[^{14}C]aminohippurate by HEK-hOAT1 (Fig. 6) and [^{3}H]estrone sulfate by HEK-hOAT3 (Fig. 7) was assessed in the absence or presence of extracellular Cl^-. With the use of a nonlinear least squares regression analysis, kinetic parameters were calculated according to the Michaelis-Menten equation in three separate experiments. Apparent Michaelis-Menten constants (K_m) and maximal uptake rate (V_{max}) values are summarized in Table 2. Substitution of gluconate with Cl^- did not change the K_m value for the uptake of *p*-[^{14}C]aminohippurate by HEK-hOAT1 but caused an approximate

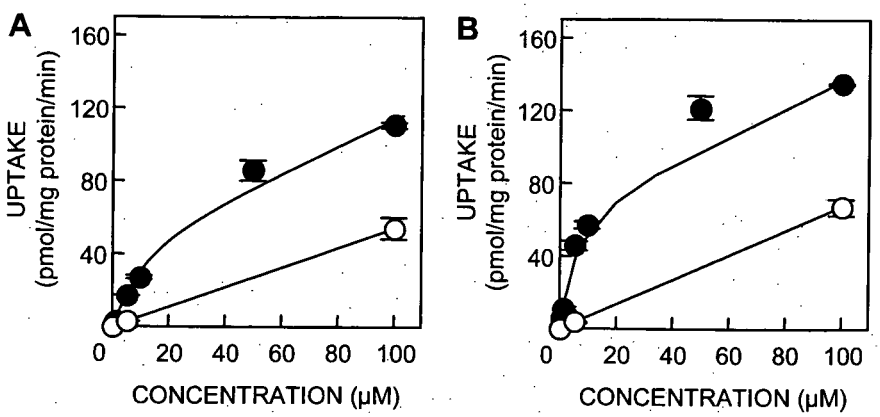

Fig. 7. Effect of extracellular Cl^- on the concentration-dependent uptake of [^{3}H]estrone sulfate by HEK-hOAT3. HEK-hOAT3 were incubated in Cl^--free (*A*) or Cl^--containing (*B*) incubation medium with various concentrations of [^{3}H]estrone sulfate in the absence (●) or presence (○) of unlabeled 1 mM estrone sulfate at 37°C for 1 min. Each point represents the mean ± SE of 3 monolayers from a typical experiment.

Table 2. *Effects of extracellular Cl^- on K_m and V_{max} values for the uptake of p-aminohippurate by HEK-hOAT1 and estrone sulfate by HEK-hOAT3*

		K_m, μM	V_{max}, pmol·mg protein^{-1}·min^{-1}
HEK-hOAT1 (*p*-aminohippurate)	Cl^- (−)	55.6±10.5	218.3±27.88
	Cl^- (+)	41.7±3.98	580.5±13.96*
HEK-hOAT3 (estrone sulfate)	Cl^- (−)	17.9±2.92	74.4±21.15
	Cl^- (+)	6.2±0.56*	90.0±9.54

Each value represents the mean ± SE of 3 separate experiments. V_{max}, maximum velocity; K_m, Michaelis-Menten constant; (−), uptake in Cl^--free incubation medium; (+), uptake in Cl^--containing incubation medium. *$P <$ 0.05, significantly different from values for uptake in Cl^--free incubation medium.

threefold increase in the V_{max} value. On the other hand, replacement of gluconate with Cl^- decreased the K_m value for the uptake of [^{3}H]estrone sulfate by HEK-hOAT3 to about one-third but did not change the V_{max} value. In addition, we evaluated the influence of Cl^- on the concentration-dependent uptake of cefotiam by HEK-hOAT3 (Fig. 8). The K_m values for the uptake of cefotiam by HEK-hOAT3 in Cl^--free and in Cl^--containing medium were 1,702.0 and 552.3 μM, respectively. The V_{max} values for the uptake in Cl^--free and in Cl^--containing medium were 146.4 and 186.9 pmol·mg protein^{-1}·15 min^{-1}, respectively. These results demonstrated that, similar to the results for the uptake of [^{3}H]estrone sulfate by HEK-hOAT3, the K_m value was decreased to approximately one-third for the uptake of cefotiam by HEK-hOAT3, while the V_{max} value was little affected.

DISCUSSION

In the human kidney, organic anion transport systems play critical roles in the excretion of organic anions. It has been described that the activities of these transport systems are regulated by inorganic anions. Chloride ion is one of the most abundant anions in the human body and has been demonstrated to affect renal tubular transport of organic anions (8, 13, 14). However, this phenomenon has not been sufficiently studied at the molecular level. In this study, we showed that both hOAT1 and hOAT3 were upregulated by Cl^-, but the effects of Cl^- on transport kinetics were different between hOAT1 and hOAT3.

Schmitt and Burckhardt (14) reported that the substitution of Cl^- with Br^- did not affect the uptake of *p*-aminohippurate by bovine renal basolateral membrane vesicles, while the replacement of Cl^- with SO_4^{2-} or gluconate decreased the uptake. Pritchard (13) also demonstrated that replacing Cl^- with SO_4^{2-} or gluconate decreased the uptake of *p*-aminohippurate by rat renal basolateral membrane vesicles. Therefore, Br^- is an effective substitute for Cl^- in basolateral organic anion transport, while SO_4^{2-} and gluconate are poor substitutes for Cl^-. In the present study, the replacement of Cl^- with Br^- had little effect on the uptake of *p*-[^{14}C]aminohippurate by HEK-hOAT1, while accumulation of *p*-[^{14}C]aminohippurate was decreased to one-half to one-third by replacing Cl^- with SO_4^{2-} or gluconate. Therefore, *p*-aminohippurate uptake by hOAT1 is highly dependent on Cl^-. Br^- could maintain the uptake as a substitute for Cl^-, but SO_4^{2-} and gluconate could not. Our results are consistent with previous studies, suggesting that hOAT1 is involved in the Cl^--dependent regulation of the basolateral transport of *p*-aminohippurate in renal proximal tubules.

In our previous examination (8), the uptake of *p*-aminohippurate by rat renal basolateral membrane vesicles was found to depend on the concentration of Cl^-, and the same result was obtained by Pritchard (13). In the present study, the uptake of *p*-[^{14}C]aminohippurate by HEK-hOAT1 and [^{3}H]estrone sulfate by HEK-hOAT3 was dependent on the concentration of Cl^- and was not saturated at 0–150 mM. Physiologically, the Cl^- concentration in blood ranges from 95 to 105 mM in healthy individuals (10). However, in patients with diseases such as acidosis and alkalosis, the plasma concentration of Cl^- can be in the range of 78–128 mM (17). On the basis of the present results, it is suggested that the activities of hOAT1 and hOAT3 are not saturated and altered with the change in the concentration of Cl^-. In addition, information is now available about the movement of Cl^- at the basolateral membranes of proximal tubules. Ishibashi et al. (9) demonstrated that a Na^+-dependent Cl^-/HCO_3^- exchanger plays a dominant role in the efflux of Cl^- at the basolateral membranes. It is implied that the Cl^- transport system controls the concentration of Cl^- around hOAT1 and hOAT3 and cooperates with hOAT1 and hOAT3. Soleimani et al. (16) indicated that the basolateral Cl^-/base exchange activity in proximal tubular cells decreased under acidic conditions and increased under alkalotic conditions. Thus it is probable that the functions of hOAT1 and hOAT3 are affected under pathological conditions such as metabolic acidosis and alkalosis.

Several studies have examined the effects of Cl^- on the transport of organic anions at basolateral membranes (8, 13, 14), but only *p*-aminohippurate was used as a substrate. In the current

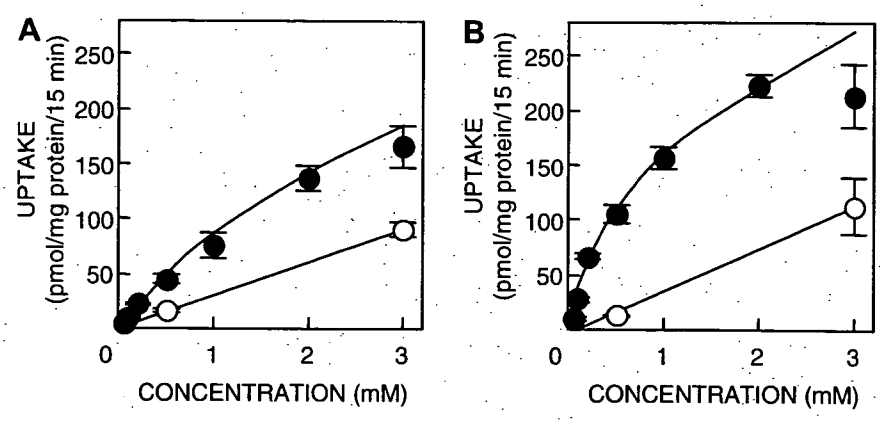

Fig. 8. Effect of extracellular Cl^- on the concentration-dependent uptake of cefotiam by HEK-hOAT3. HEK-hOAT3 were incubated in Cl^--free (*A*) or Cl^--containing (*B*) incubation medium with various concentrations of cefotiam in the absence (●) or presence (○) of 1 mM probenecid at 37°C for 15 min. Each point represents the mean ± SE of 3 monolayers from a typical experiment.

study, the uptake of various compounds by hOAT1 and hOAT3 was increased by Cl^-. These results indicated that Cl^- affects both hOAT1 and hOAT3, and these effects are not dependent on the substrates. It has been shown that hOAT1 and hOAT3 are involved in the basolateral uptake of various drugs including diuretics, antiviral drugs, and cephalosporin antibiotics (5, 20, 21). Therefore, it is implied that the basolateral uptake of these drugs from blood circulation into tubular cells is regulated by Cl^-.

It has been shown that OAT1 and OAT3 are organic anion/dicarboxylate exchangers (18, 19), and organic anion transport into the cells by these transporters is undertaken in exchange for endogenous dicarboxylate, α-KG. Thus intracellular concentration of α-KG is a major determinant of the transport activities of hOAT1 and hOAT3. In the current study, we showed that Cl^- had no effect on intracellular α-KG concentration. It was suggested that the change of intracellular concentration of α-KG is not associated with the effects of Cl^- on the functions of hOAT1 and hOAT3.

Previously, we demonstrated that *p*-aminohippurate uptake by rat renal basolateral membrane vesicles was stimulated by the increase in Cl^- concentration, when the concentration of Cl^- in the vesicles was equal to that on the outside (8). In the current study, the uptake of *p*-aminohippurate by HEK-hOAT1 and estrone sulfate by HEK-hOAT3 was dependent on extracellular Cl^- concentration, and these phenomena were also observed when there were no concentration gradients of Cl^- across plasma membranes. Therefore, it is reasonable to assume that Cl^- outside of the cells, i.e., the same side as the substrate, upregulates the activities of hOAT1 and hOAT3.

Subsequently, the influences of extracellular Cl^- on the kinetic parameters of transport via hOAT1 and hOAT3 were examined. When gluconate was substituted with Cl^-, the V_{max} value for the uptake of *p*-aminohippurate by hOAT1 was increased about threefold without a significant effect on the K_m value. On the other hand, under the same conditions, the K_m values for the hOAT3-mediated uptake of estrone sulfate and cefotiam were decreased to approximately one-third without any effect on V_{max} values. These results suggested that Cl^- participates in the *trans*-location rate for the uptake of *p*-aminohippurate by hOAT1 and in the substrate affinity for the uptake of estrone sulfate and cefotiam by hOAT3. The substrate recognition of hOAT1 is different from that of hOAT3. For example, hOAT1 efficiently transports the nucleotide antivirals adefovir, cidofovir, and tenofovir (22), whereas hOAT3 transports cephalosporin antibiotics (21). Therefore, at basolateral membranes, Cl^- affects V_{max} values for the uptake of nucleotide antivirals or K_m values for the uptake of cephalosporin antibiotics. Although how Cl^- affects the activities of hOAT1 and hOAT3 is unclear, it was indicated that the transport activities of hOAT1 and hOAT3 are upregulated in a different manner by Cl^-.

In summary, Cl^--dependent regulation of hOAT1 and hOAT3 was examined in detail for the first time. It was suggested that Cl^- is involved in the regulation and maintenance of organic anion secretion in renal proximal tubules. In addition, the effects of Cl^- on transport kinetics differ between hOAT1 and hOAT3, suggesting that Cl^- participates in the *trans*-location process for hOAT1 and the substrate recognition process for hOAT3.

GRANTS

This work was supported in part by a grant-in-aid for Research on Advanced Medical Technology from the Ministry of Health, Labor and Welfare of Japan, by a grant-in-aid for Scientific Research from the Ministry of Education, Science, Culture and Sports of Japan, and by the 21st Century COE program "Knowledge Information Infrastructure for Genome Science." H. Ueo was supported as a teaching assistant by the 21st Century Center of Excellence program "Knowledge Information Infrastructure for Genome Science."

REFERENCES

1. **Bradford MM.** A rapid and sensitive method for the quantitation of microgram quantities of protein utilizing the principle of protein-dye binding. *Anal Biochem* 72: 248–254, 1976.
2. **Burckhardt G, Wolff NA.** Structure of renal organic anion and cation transporters. *Am J Physiol Renal Physiol* 278: F853–F866, 2000.
3. **Cha SH, Sekine T, Fukushima J, Kanai Y, Kobayashi Y, Goya T, Endou H.** Identification and characterization of human organic anion transporter 3 expressing predominantly in the kidney. *Mol Pharmacol* 59: 1277–1286, 2001.
4. **Chao AC, Dix JA, Sellers MC, Verkman AS.** Fluorescence measurement of chloride transport in monolayer cultured cells. Mechanisms of chloride transport in fibroblasts. *Biophys J* 56: 1071–1081, 1989.
5. **Hasannejad H, Takeda M, Taki K, Shin HJ, Babu E, Jutabha P, Khamdang S, Aleboyeh M, Onozato ML, Tojo A, Enomoto A, Anzai N, Narikawa S, Huang XL, Niwa T, Endou H.** Interactions of human organic anion transporters with diuretics. *J Pharmacol Exp Ther* 308: 1021–1029, 2004.
6. **Hosoyamada M, Sekine T, Kanai Y, Endou H.** Molecular cloning and functional expression of a multispecific organic anion transporter from human kidney. *Am J Physiol Renal Physiol* 276: F122–F128, 1999.
7. **Inui K, Masuda S, Saito H.** Cellular and molecular aspects of drug transport in the kidney. *Kidney Int* 58: 944–958, 2000.
8. **Inui K, Takano M, Okano T, Hori R.** Role of chloride on carrier-mediated transport of *p*-aminohippurate in rat renal basolateral membrane vesicles. *Biochim Biophys Acta* 855: 425–428, 1986.
9. **Ishibashi K, Rector FC Jr, Berry CA.** Role of Na^+-dependent Cl^-/HCO_3^- exchange in basolateral Cl^- transport of rabbit proximal tubules. *Am J Physiol Renal Fluid Electrolyte Physiol* 264: F251–F258, 1993.
10. **Koch SM, Taylor RW.** Chloride ion in intensive care medicine. *Crit Care Med* 20: 227–240, 1992.
11. **Krapf R, Berry CA, Verkman AS.** Estimation of intracellular chloride activity in isolated perfused rabbit proximal convoluted tubules using a fluorescent indicator. *Biophys J* 53: 955–962, 1988.
12. **Motohashi H, Sakurai Y, Saito H, Masuda S, Urakami Y, Goto M, Fukatsu A, Ogawa O, Inui K.** Gene expression levels and immunolocalization of organic ion transporters in the human kidney. *J Am Soc Nephrol* 13: 866–874, 2002.
13. **Pritchard JB.** Coupled transport of *p*-aminohippurate by rat kidney basolateral membrane vesicles. *Am J Physiol Renal Fluid Electrolyte Physiol* 255: F597–F604, 1988.
14. **Schmitt C, Burckhardt G.** Modulation by anions of *p*-aminohippurate transport in bovine renal basolateral membrane vesicles. *Pflügers Arch* 425: 241–247, 1993.
15. **Sekine T, Cha SH, Endou H.** The multispecific organic anion transporter (OAT) family. *Pflügers Arch* 440: 337–350, 2000.
16. **Soleimani M, Hattabaugh YJ, Bizal GL.** Acute regulation of Na^+/H^+ exchange, $Na^+:HCO_3^-$ cotransport, and Cl^-/base exchange in acid base disorders. *J Lab Clin Med* 124: 69–78, 1994.
17. **Story DA, Morimatsu H, Bellomo R.** Hyperchloremic acidosis in the critically ill: one of the strong-ion acidoses? *Anesth Analg* 103: 144–148, table of contents, 2006.
18. **Sweet DH, Chan LM, Walden R, Yang XP, Miller DS, Pritchard JB.** Organic anion transporter 3 (*Slc22a8*) is a dicarboxylate exchanger indirectly coupled to the Na^+ gradient. *Am J Physiol Renal Physiol* 284: F763–F769, 2003.
19. **Sweet DH, Wolff NA, Pritchard JB.** Expression cloning and characterization of ROAT1. The basolateral organic anion transporter in rat kidney. *J Biol Chem* 272: 30088–30095, 1997.
20. **Takeda M, Khamdang S, Narikawa S, Kimura H, Kobayashi Y, Yamamoto T, Cha SH, Sekine T, Endou H.** Human organic anion transporters and human organic cation transporters mediate renal antiviral transport. *J Pharmacol Exp Ther* 300: 918–924, 2002.
21. **Ueo H, Motohashi H, Katsura T, Inui K.** Human organic anion transporter hOAT3 is a potent transporter of cephalosporin antibiotics, in comparison with hOAT1. *Biochem Pharmacol* 70: 1104–1113, 2005.
22. **Uwai Y, Ida H, Tsuji Y, Katsura T, Inui K.** Renal transport of adefovir, cidofovir, and tenofovir by SLC22A family members (hOAT1, hOAT3 and hOCT2). *Pharm Res* 24: 811–815, 2007.
23. **Williamson JR, Corkey BE.** Assay of citric acid cycle intermediates and related compounds–update with tissue metabolite levels and intracellular distribution. *Methods Enzymol* 55: 200–222, 1979.

Int J Clin Oncol (2007) 12:284–290
DOI 10.1007/s10147-007-0681-y

ORIGINAL ARTICLE

Mari Jiko · Ikuko Yano · Eriko Sato
Kazushige Takahashi · Hideyuki Motohashi
Satohiro Masuda · Masahiro Okuda · Noriyuki Ito
Eijiro Nakamura · Takehiko Segawa · Toshiyuki Kamoto
Osamu Ogawa · Ken-ichi Inui

Pharmacokinetics and pharmacodynamics of paclitaxel with carboplatin or gemcitabine, and effects of *CYP3A5* and *MDR1* polymorphisms in patients with urogenital cancers

Received: March 1, 2007 / Accepted: April 12, 2007

Abstract
Background. We investigated the pharmacokinetics and pharmacodynamics of paclitaxel with carboplatin or gemcitabine in patients with urogenital cancer to clarify the significance of monitoring of the serum concentration of paclitaxel.
Methods. Paclitaxel was administered at 175 mg/m^2 or 150 mg/m^2 to patients with hormone-refractory prostate cancer (n = 10) or advanced transitional cell carcinoma (n = 6) along with carboplatin or gemcitabine, respectively. The relationships between pharmacokinetic parameters and hematological adverse effects, as well as pharmacological effects, were examined. The effects of patient characteristics, including single-nucleotide polymorphisms of *MDR1(ABCB1)*, *CYP2C8*, *CYP3A4*, and *CYP3A5*, on the total body clearance of paclitaxel were evaluated.
Results. Total body clearance and volume of distribution at a steady-state after the intravenous infusion of paclitaxel were not significantly different between patients with carboplatin or gemcitabine. The percent decreases in neutrophils and platelets for the regimen with gemcitabine were significantly greater than those with carboplatin, and showed a significant positive relationship with the observed concentration at the end of infusion or time above 0.1-μM concentration of paclitaxel. Post-therapy decreases in prostate-specific antigen were not positively correlated with the extent of paclitaxel exposure in the prostate cancer patients. Neither the polymorphisms at exon 26 (C3435T) and at exon 21 (G2677A/T) in *MDR1* nor the *CYP3A5*1* allele significantly affected the total body clearance of paclitaxel.
Conclusion. The hematological side effects of paclitaxel were intensified by gemcitabine, and were correlated with paclitaxel pharmacokinetics. Monitoring of the serum concentration of paclitaxel will facilitate the therapy, with less myelosuppression and without any loss of therapeutic efficacy.

Key words Paclitaxel · Pharmacokinetics · Pharmacodynamics · Carboplatin · Gemcitabine

M. Jiko · I. Yano · E. Sato · K. Takahashi · H. Motohashi · S. Masuda · M. Okuda · K. Inui (✉)
Department of Pharmacy, Kyoto University Hospital, Faculty of Medicine, Kyoto University, Sakyo-ku, Kyoto 606-8507, Japan
Tel. +81-75-751-3577; Fax +81-75-751-4207
e-mail: inui@kuhp.kyoto-u.ac.jp

N. Ito · E. Nakamura · T. Segawa · T. Kamoto · O. Ogawa
Department of Urology, Graduate School of Medicine, Kyoto University, Kyoto, Japan

Introduction

Paclitaxel, a taxane anticancer drug, which stabilizes microtubule polymerization, leading to mitotic arrest, is used to treat several cancers, such as ovarian, breast and non-small cell lung cancers.[1,2] Furthermore, recent studies have shown that paclitaxel has an effect on hormone-refractory prostate cancer and advanced transitional cell carcinoma of the urothelial tract.[3,4] Dosages of anticancer drugs including taxanes are usually determined based on the body surface area of individual patients. However, these agents have strong toxicity even when they are administered properly, and the interindividual variability of pharmacokinetics might account for the unpredictable toxicity. Gianni et al.[5] and Ohtsu et al.[6] reported that neutropenia was related to the length of exposure to a paclitaxel concentration above 0.05 μM. Moreover, the rate of survival among patients with non-small cell lung cancer was reported to correlate with the period of exposure to 0.1 μM or more of paclitaxel.[7] These reports suggested that the serum concentration of paclitaxel was related to both adverse effects and clinical outcome. Regarding the relationship between patient characteristics and paclitaxel pharmacokinetics, the alanine aminotransferase level was reported to correlate with paclitaxel clearance.[7] In the case of another taxane, docetaxel, Bruno et al.[8] reported that α_1-acid glycoprotein and bilirubin levels correlated with the clearance of this drug. Therefore, it is possible that dosage adjustment based on the characteristics of each patient would bring about less toxic therapy without a reduction in pharmacological effect.

Single-nucleotide polymorphisms (SNPs) of drug-metabolizing enzymes or drug transporters are reported to contribute to the pharmacokinetic variability of several drugs.[9] Paclitaxel is metabolized by the cytochrome P450 (CYP) 3A subfamily and CYP2C8 in the liver, and is also a substrate of P-glycoprotein, the encoded product of the human *MDR1* (*ABCB1*) gene.[10,11] CYP3A5, a homolog of CYP3A4, overlaps greatly in its substrate specificity with CYP3A4. Goh et al.[12] reported that, in *CYP3A5*3* homozygotes, midazolam clearance was lower than that in patients with the *1 allele, but docetaxel clearance did not differ from that in patients with *CYP3A5*1*, although both midazolam and docetaxel are metabolized by CYP3A4 and CYP3A5.[13] We have reported that the mRNA level of CYP3A5 was significantly reduced by the *3/*3 genotype, and the concentration/oral dose ratio of tacrolimus was decreased in recipients engrafted with partial liver carrying the *CYP3A5*1/*1* genotype.[14] Of note, a relationship between SNPs of the *MDR1* gene and the expression/function of MDR1 has been reported by several investigators. Hoffmeyer et al.[15] reported that humans homozygous for a polymorphism at exon 26 (C3435T) had significantly lower duodenal MDR1 levels and the highest plasma digoxin levels after oral administration. G2677T/A at exon 21, which is strongly linked to the C3435T transition at exon 26, alters the disposition of the known P-glycoprotein substrate fexofenadine.[16] We reported that ten *MDR1* SNPs, including C3435T and G2677T/A, did not influence the intestinal expression level of MDR1 mRNA or the tacrolimus concentration/dose ratio in living-donor liver transplant patients.[17] Thus, the effect of *MDR1* genotypes on the expression and transport activity of MDR1 is under discussion. For *CYP2C8*, Dai et al.[18] reported that alleles *2 and *3 had a smaller clearance of paclitaxel. At present, there are a few reports about the relation between paclitaxel pharmacokinetics and polymorphisms of *CYP3A4*, *CYP3A5*, and *MDR1*.[19,20]

In this study, we examined the pharmacokinetics and pharmacodynamics of paclitaxel in patients with carboplatin or gemcitabine to clarify the usefulness of monitoring the serum drug concentration. In addition, the effect of patient characteristics, including SNPs of *CYPs* and *MDR1* on the pharmacokinetics of paclitaxel was evaluated.

Patients and methods

Patient selection

Patients who were treated with paclitaxel for hormone-refractory prostate cancer ($n = 10$) or advanced transitional cell carcinoma ($n = 6$) at the Department of Urology, Kyoto University Hospital, between March 2003 and December 2004 were enrolled in this study. The study was conducted during the first cycle of chemotherapy with paclitaxel. The study was performed in accordance with the Declaration of Helsinki and its amendments, and was approved by the Kyoto University Graduate School and Faculty of Medicine Ethics Committee. Written informed consent was obtained from each patient. The characteristics and clinical data of patients are summarized in Table 1.

Chemotherapy regimen and study protocol

Paclitaxel (Taxol; Bristol-Myers Squibb, Tokyo, Japan) for clinical use was provided as a concentrated sterile solution (6 mg/ml) in a 5-ml vial in a mixture of cremophor EL and dehydrated alcohol (1: 1 vol/vol). This product was diluted before use with 500 ml of a 5% glucose solution. Paclitaxel was administered at 175 mg/m^2 and 150 mg/m^2, as a 3-h continuous intravenous infusion, for prostate cancer and transitional cell carcinoma, respectively.

Premedication consisted of a histamine H_2 antagonist, chlorpheniramine maleate, and dexamethasone was intravenously administered 30 min before the infusion of paclitaxel. The administration of paclitaxel (175 mg/m^2) was followed by carboplatin, given as a 150-min infusion, for the patients with prostate cancer. The dose of carboplatin was

Table 1. Characteristics and biochemical parameters of patients before the administration of paclitaxel with carboplatin or gemcitabine

	Carboplatin ($n = 10$)	Gemcitabine ($n = 6$)
Age (years)	64.9 ± 6.0	67.8 ± 8.8
Body weight (kg)	66.6 ± 6.3	53.4 ± 2.3
White blood cells (×10^3/μl)	7.47 ± 2.53	6.92 ± 1.67
Neutrophils (×10^3/μl)	5.32 ± 2.25	4.80 ± 1.38
Platelets (×10^3/μl)	200 ± 44	278 ± 98
Aspartate aminotransferase (IU/l)	19.0 ± 5.1	20.7 ± 7.3
Alanine aminotransferase (IU/l)	16.9 ± 5.9	23.3 ± 7.6
Total bilirubin (mg/dl)	0.64 ± 0.25	0.55 ± 0.16
Albumin (g/dl)	4.05 ± 0.33	4.07 ± 0.22
Total cholesterol (mg/dl)	190 ± 28	199 ± 53
Serum triglyceride (mg/dl)	181 ± 61	192 ± 50
Blood urea nitrogen (mg/dl)	16.2 ± 8.2	16.0 ± 2.37
Creatinine clearance (ml/min)	50.3 ± 14.2	34.4 ± 11.4*
Prostate-specific antigen (ng/ml)	216 ± 424	ND

*$P < 0.05$, significantly different from the mean value in the carboplatin group
Values are means ± SD
ND, not determined

determined based on the Calvert formula,[21] with a target area under the concentration-time curve of 5 mg/min × ml. All patients received 560 mg estramustine phosphate daily, given orally. In the patients with transitional cell carcinoma, the administration of paclitaxel (150 mg/m^2) was followed by gemcitabine (2500 mg/m^2).[4] Serum samples for paclitaxel pharmacokinetics were obtained before, at the end of, and 1, 2, 6, 24, and 48 h after the infusion of paclitaxel. Blood cell counts were measured twice per week for 2 weeks after the administration of paclitaxel, and monitored until the hematological values recovered to the normal ranges. The serum prostate-specific antigen (PSA) concentration was measured every 2 weeks.

Analysis of paclitaxel and genotyping of *MDR1*, *CYP2C8*, *CYP3A4*, and *CYP3A5*

Paclitaxel was extracted from serum samples using a Sep-pak C_{18} column (Waters, Bedford, MA, USA) as described previously.[22] The concentration of paclitaxel was measured by high-performance liquid chromatography.[22] The lower limit of determination for paclitaxel was 0.01 μg/ml. The calibration curve was linear over the range of 0.01 to 10 μg/ml ($r^2 > 0.99$). The intraassay precision was 9.8%, 3.8%, and 0.8% for the concentrations of 0.01, 0.1, and 1 μg/ml, respectively. Genomic DNA was isolated from blood samples with a PAXgene Blood DNA kit (PreAnalytiX, Hombrechtikon, Switzerland). The genotypes of the *MDR1*, *CYP2C8*, *CYP3A4*, and *CYP3A5* genes were investigated by polymerase chain reaction (PCR)-restriction enzyme fragment length polymorphism. The specific primers and restriction enzymes used in this study were as described previously. C3435T and G2677T/A polymorphisms were examined based on the method of Goto et al.[17] *CYP2C8**2 and *3 were examined according to the method of Dai et al.[18] *CYP3A4**1B and *3 and *CYP3A5**3 were examined according to the method of van Shaik et al.[23–25]

Pharmacokinetic and pharmacodynamic analyses

A conventional two-compartment model was used to analyze the serum concentration-time profiles after the intravenous administration of paclitaxel, with the ordinary nonlinear least squares method (double precision NONMEM Version V; GloboMax LLC, Hanover, MD, USA).[26] The C_{max} value was the observed concentration at the end of infusion. The area under the serum concentration-time curve (AUC) after intravenous administration was calculated by dividing the dose by the calculated total body clearance. The time above paclitaxel concentration 0.05 μM ($T > 0.05$ μM) and the time above paclitaxel concentration 0.1 μM ($T > 0.1$ μM) were graphically measured. The influence of patient characteristics as well as genotypes on the pharmacokinetic parameters of paclitaxel was investigated.

Hematological toxicity was evaluated as nadir and percent decrease (% decrease) against the pretreatment values for white blood cell, absolute neutrophil, or platelet counts. The percent decrease was calculated by the following equation:

$$\%\text{Decrease} = \frac{\text{pretreatment-nadir}}{\text{pretreatment}} \times 100$$

Outcomes of chemotherapy for prostate cancer were assessed independently using post-therapy changes in the PSA concentration. We evaluated the relationship between the pharmacokinetic parameters (C_{max}, AUC, $T > 0.1$ μM, and $T > 0.05$ μM) of paclitaxel and hematological toxicity, as well as therapeutic response.

Statistical analysis

Data values are presented as means ±SD. The statistical significance of differences in mean values between two groups was analyzed using the nonpaired *t*-test, if the variances in each group were similar, otherwise the Mann-Whitney *U*-test was used. Comparisons of mean values between three groups were performed using one-way analysis of variance with the post-hoc Dunnett test. Correlations between variables were examined using univariate analysis. A *P* value of less than 0.05 was considered to be significant. Statistical analyses were performed using the statistical software package Statview version 5.0 (Abacus Concepts, Berkeley, CA, USA).

Results

Patient characteristics

All patients enrolled in this study were relatively old (age, 55–77 years) men. The characteristics in patients with carboplatin and those with gemcitabine were not significantly different, except for creatinine clearance (Table 1). There was no patient with hepatic impairment. No patient was treated with medicines known as strong inhibitors or inducers of CYP3A4 or P-glycoprotein.

Paclitaxel pharmacokinetics

Although there was large interindividual variability in the serum concentration of paclitaxel after intravenous infusion, values in each patient well fitted a two-compartmental model (Fig. 1). Table 2 shows the pharmacokinetic parameters of paclitaxel in patients with carboplatin or gemcitabine. The coefficient of variation (CV%) for each parameter was 29% to 52% with carboplatin, and 24% to 70% with gemcitabine. The central volume of distribution for paclitaxel was significantly larger in patients with gemcitabine than in those with carboplatin. The C_{max}, AUC, $T > 0.1$ μM, and $T > 0.05$ μM were not significantly different between the two groups in spite of the dosage difference, because of the large interindividual variability.

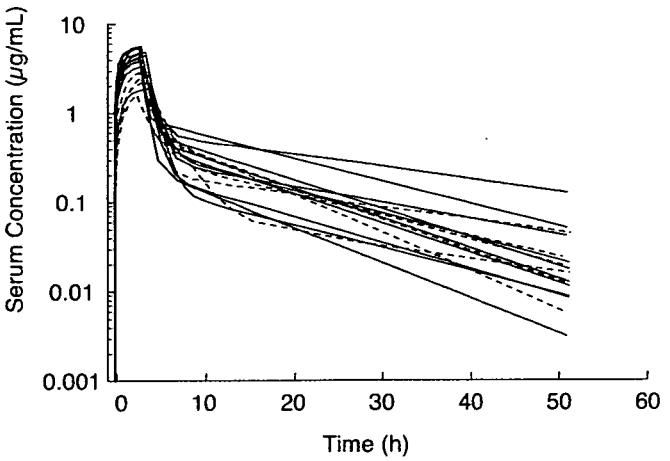

Fig. 1. Serum concentration-time curves of paclitaxel in patients with carboplatin (n = 10) or gemcitabine (n = 6). The *solid lines* show the serum concentrations after paclitaxel administration (175 mg/m^2) with carboplatin in each prostate cancer patient, and the *dotted lines* show the serum concentrations after paclitaxel administration (150 mg/m^2) with gemcitabine in each patient with advanced transitional cell carcinoma. *Each line* was obtained by the nonlinear least squares method, using the measured serum paclitaxel concentration after the intravenous infusion of the drug

Table 2. Pharmacokinetic parameters of paclitaxel after intravenous infusion in patients with carboplatin or gemcitabine

Parameter	Carboplatin	Gemcitabine
CL (l/h per m^2)	9.00 ± 3.48	9.79 ± 2.81
Q (l/h per m^2)	4.40 ± 1.47	6.72 ± 4.68
V_1 (l/m^2)	9.65 ± 4.18	22.0 ± 14.5*
V_{ss} (l/m^2)	57.8 ± 24.5	93.7 ± 35.9
C_{max} (μg/ml)	4.77 ± 1.38	3.37 ± 1.72
AUC (μg/h × ml)	22.0 ± 8.0	16.7 ± 5.8
T > 0.1 μM (h)	27.1 ± 14.1	23.6 ± 6.6
T > 0.05 μM (h)	38.0 ± 11.6	35.0 ± 8.5

* $P < 0.05$, significantly different from the mean value in the carboplatin group

Values are means ± SD

CL, total body clearance; Q, intercompartmental clearance; V_1, central volume of distribution; V_{ss}, volume of distribution at a steady-state; C_{max}, observed maximum concentration; AUC, area under the concentration-time curve; T > 0.1 μM, time above serum paclitaxel concentration 0.1 μM; T > 0.05 μM, time above serum paclitaxel concentration 0.05 μM

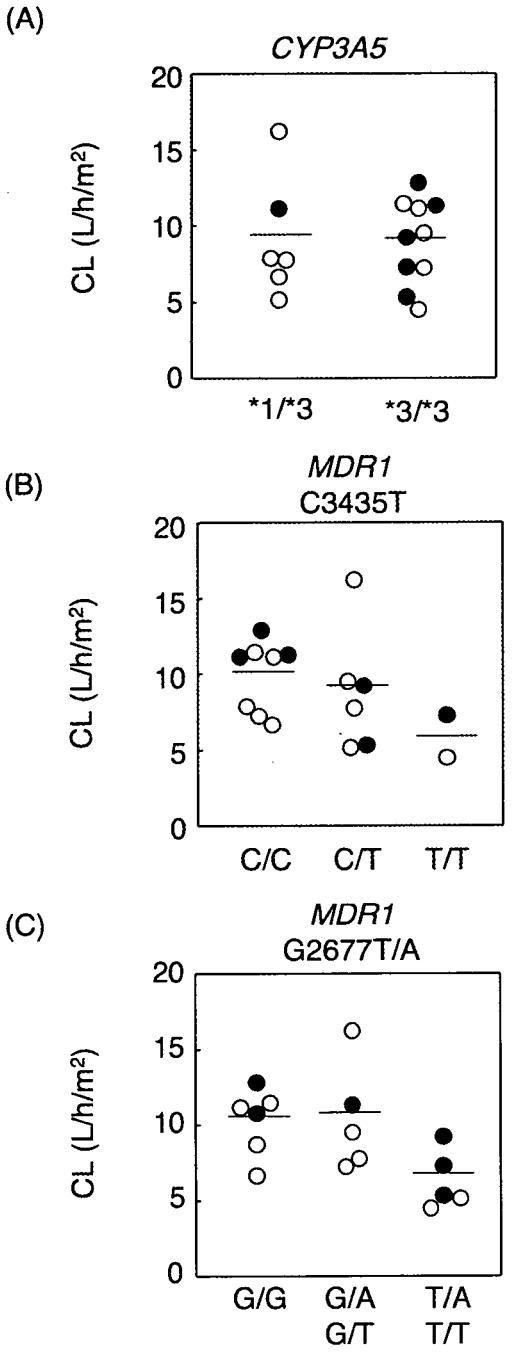

Fig. 2A–C. Effects of genetic polymorphisms of **A** *CYP3A5**3, **B** *MDR1* C3435T, and **C** *MDR1* G2677T/A on paclitaxel clearance (*CL*). The *bars* show the mean values of paclitaxel clearance in each group. The *open and closed symbols* represent the data for patients with carboplatin and gemcitabine, respectively

Effect of patient characteristics and genotype on paclitaxel clearance

The clearance of paclitaxel in each patient correlated negatively, but not significantly, with alanine aminotransferase (r^2 = 0.230; P = 0.0602). None of the other biochemical parameters tested (aspartate aminotransferase, total bilirubin, albumin, total cholesterol, serum triglyceride, blood urea nitrogen, and creatinine clearance) showed a significant relationship with paclitaxel clearance. The clearance of paclitaxel in patients who had the *CYP3A5**1/*3 genotype was not significantly different from that in those who had the *CYP3A5**3/*3 genotype (Fig. 2A). For the genotypes at exon 26 (C3435T) in *MDR1*, statistical analysis of differences in clearance values between genotypic groups were not performed because of the small sample size (Fig. 2B). For genotypes at exon 21 (G2677T/A), homozygotes, namely the subjects with T/A and T/T, tended to have lower paclitaxel clearance values than the G/G subjects, but the difference did not reach statistical significance (Fig. 2C). *CYP3A4**1B, *CYP3A4**3, *CYP2C8**2, and *CYP2C8**3 alleles were not detected in our patients.

Pharmacodynamic analysis

Hematological toxicity was relatively mild in this study, and only one patient showed leukopenia and neutropenia of grade 4 according to the National Cancer Institute common toxicity criteria version 2.0. The mean percent decreases in neutrophils and platelets after the intravenous administration of paclitaxel were significantly greater in patients with gemcitabine than in those with carboplatin (Table 3). The percent decrease in neutrophils was positively related with the C_{max} in patients with gemcitabine ($r^2 = 0.903$; $P = 0.002$; Fig. 3A). In addition, the percent decrease in platelets also correlated positively with the T > 0.1 μM in patients with gemcitabine ($r^2 = 0.769$; $P = 0.018$; Fig. 3B). Other pharmacokinetic parameters examined did not show a significant relationship with the nadir or percent decrease in white blood cells, neutrophils, or platelets. For the therapeutic response, the percent decrease in PSA had a tendency toward a negative relationship with C_{max}, AUC, T > 0.1 μM, and T > 0.05 μM in prostate cancer patients (C_{max}, $r^2 = 0.426$; $P = 0.039$; AUC, $r^2 = 0.248$, $P = 0.149$; T > 0.1 μM, $r^2 = 0.179$, $P = 0.233$; T > 0.05 μM, $r^2 = 0.059$, $P = 0.514$; Fig. 3C, D).

Table 3. Hematological toxicity after intravenous infusion of paclitaxel with carboplatin or gemcitabine

	Carboplatin	Gemcitabine
White blood cells		
Nadir (×10³/μl)	3.91 ± 1.96	2.52 ± 0.82
Percent decrease	47.0 ± 20.5	63.1 ± 10.3
Neutrophils		
Nadir (×10³/μl)	2.52 ± 1.60	1.26 ± 0.41
Percent decrease	50.5 ± 25.8	72.6 ± 9.0*
Platelets		
Nadir (×10³/μl)	180 ± 80	131 ± 47
Percent decrease	21.9 ± 14.5	50.1 ± 18.5*

* $P < 0.05$, significantly different from the mean value in the carboplatin group
Values are means ± SD

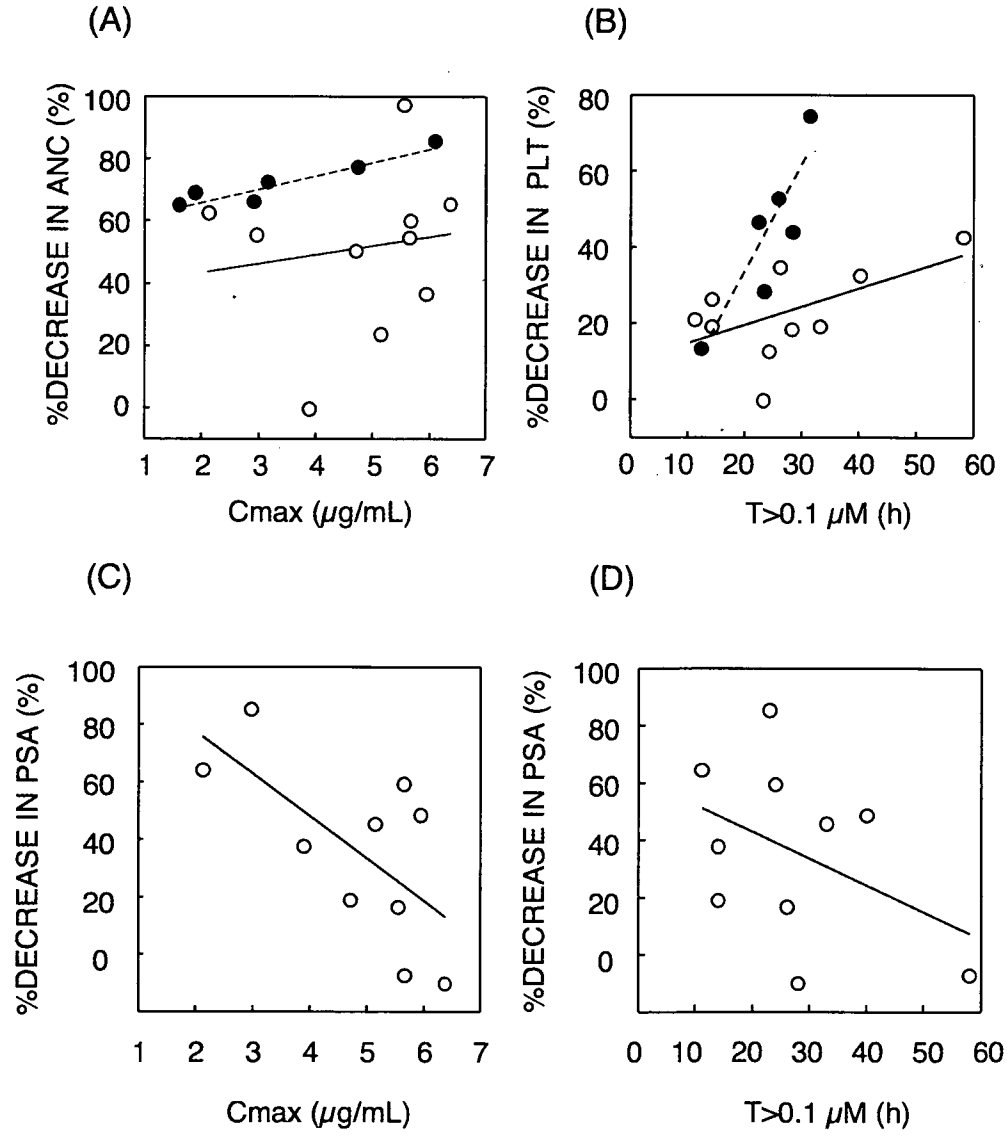

Fig. 3A–D. Relationship between the pharmacokinetic parameters of paclitaxel and hematological toxicity and therapeutic response. **A** The observed concentration at the end of infusion (C_{max}) versus percent decrease in absolute neutrophil count (*ANC*). **B** The time above paclitaxel concentration 0.1 μM ($T > 0.1 \mu M$) versus percentage decrease in platelet count (*PLT*). **C** The C_{max} versus percent decrease in prostate-specific antigen (*PSA*). **D** The T > 0.1 μM versus percentage decrease in PSA. The *open symbols* represent the data in patients with carboplatin (**A** $r^2 = 0.023$, $P = 0.689$; **B** $r^2 = 0.308$, $P = 0.098$; **C** $r^2 = 0.426$, $P = 0.039$; **D** $r^2 = 0.179$, $P = 0.233$) and the *closed symbols* represent the data in patients with gemcitabine (**A** $r^2 = 0.903$, $P = 0.002$; **B** $r^2 = 0.769$, $P = 0.018$)

Discussion

Paclitaxel is one of the most useful anticancer drugs for solid tumors such as non-small cell lung cancer or breast cancer, although it can cause severe hematological toxicity and other adverse effects. In this study, we examined the pharmacokinetics and pharmacodynamics of paclitaxel in patients with carboplatin or gemcitabine to clarify the usefulness of monitoring the serum drug concentration.

Paclitaxel disposition has often been described in terms of a saturable process,[5-7,27] but the data in our study were sufficiently fitted to a linear two-compartment model due to the relatively small dosage range. In fact, the total body clearance and volume of distribution at a steady state after intravenous paclitaxel infusion did not differ significantly between the two groups treated with paclitaxel at 175 mg/m^2 with carboplatin or at 150 mg/m^2 with gemcitabine. It has been reported that neither gemcitabine nor carboplatin affects the pharmacokinetics of paclitaxel,[7,28] which was consistent with our results. The pharmacokinetic parameters reported here also correspond to previously reported values.[19,27] Because the interindividual variability in the total body clearance of paclitaxel was as large as 39% in patients with carboplatin and 29% in patients with gemcitabine, we next examined the relationship between the characteristics of the patients and clearance values. There were no patients with hepatic dysfunction, and we did not observe a significant relationship between results of hepatic function tests such as alanine aminotransferase and clearance. However, taking into consideration that the clearance of paclitaxel tended to be negatively correlated with alanine aminotransferase and was significantly decreased in rats with hepatic failure,[22] care should be taken in the administration of paclitaxel to patients with hepatic failure. In patients with end-stage renal disease, the clearance of erythromycin, a substrate of CYP3A4, was 28% lower than that in healthy subjects.[29] Based on this finding, renal failure might affect the clearance of paclitaxel, but there was no relationship between renal function and paclitaxel clearance in this study, similar to the results obtained with our chronic renal failure model.[22] Although paclitaxel was reported to mainly bind to albumin,[30] the serum albumin concentration did not affect the pharmacokinetics of paclitaxel in this study, probably due to the small interindividual variability of albumin concentration.

The variability in the pharmacokinetics of paclitaxel was also examined by genotyping *MDR1*, *CYP2C8*, *CYP3A4*, and *CYP3A5*. The proteins encoded by these genes possibly affect the pharmacokinetics, because they are metabolizing enzymes and transporters of paclitaxel in humans. In the present study, polymorphisms at exon 21 (G2677T/A) and at exon 26 (C3435T) in *MDR1* did not significantly affect the clearance of paclitaxel. Recent reports have also shown that variant alleles in the *MDR1* gene did not explain the interindividual variability in paclitaxel pharmacokinetics.[19,20] We previously reported that no polymorphism of *MDR1* correlated with the expression of MDR1 mRNA in the intestine and kidney cortex.[17,31] According to a recent metaanalysis of the influence of the *MDR1* C3435T polymorphism, this SNP does not affect the pharmacokinetics of digoxin or the expression of MDR1 mRNA.[32] Shon et al.[33] reported that, after itraconazole pretreatment, the oral clearance of fexofenadine in subjects with the haplotype 2677TT/3435TT was lower than that in 2677GG/3435CC subjects, although there was no significant difference in the placebo phase. Unfortunately, in the present study, we could not evaluate the effects of *MDR1* haplotypes on the pharmacokinetics of paclitaxel, because of the small sample size. Based on these findings, issues relating to *MDR1* haplotypes, environmental factors, and study design might confound the observed effects of *MDR1* polymorphisms on drug disposition in vivo. Of note, patients who had the *CYP3A5**1/*3 genotype did not show a larger clearance of paclitaxel than those with the *CYP3A5**3/*3 genotype, consistent with previous results for paclitaxel.[20] In the case of paclitaxel, because CYP2C8 as well as CYP3A4 was reported to be a major metabolizing enzyme, the genotype of *CYP3A5* might have little contribution to the pharmacokinetics of paclitaxel. We could not find any patients with the *CYP2C8**2 and *3 or *CYP3A4**1B and*3 alleles, which were reported to be rare in Japanese.[14,34]

The percent decreases in neutrophils and platelets were significantly greater for the regimen with gemcitabine than for the regimen with carboplatin, although the parameters of paclitaxel exposure such as C_{max}, AUC, $T > 0.1\,\mu M$, and $T > 0.05\,\mu M$ were not significantly different between the two groups. In addition, the percent decrease in neutrophils and that in platelets had a significant positive relationship with the C_{max} and $T > 0.1\,\mu M$ of paclitaxel, respectively, in patients with gemcitabine. Because the total dose of gemcitabine was as large as 2500 mg/m^2 in the present study, we considered that the hematological toxicity increased due to the synergism of paclitaxel and gemcitabine, and that greater paclitaxel exposure intensified the decrease of neutrophils and platelets by gemcitabine. Interestingly, the pharmacological effect, which was assessed as the percent decrease in PSA in prostate cancer patients, had a tendency toward a negative correlation with the C_{max}, AUC, $T > 0.1\,\mu M$, and $T > 0.05\,\mu M$ of paclitaxel. In vitro, in human non-small cell lung carcinoma A549 cells, a paclitaxel concentration higher than 9 nM blocked the cell cycle in the G2-M phase, resulting in cell death.[35] Jordan et al.[36] also reported that the proliferation of HeLa cells was blocked half-maximally by paclitaxel at a concentration of 8 nM, and inhibition was complete at concentrations above 33 nM. Of interest, microtubule-depolymerizing agents exhibited a biphasic dose-response curve, with mitotic arrest at low drug concentrations that failed to depolymerize microtubules, and a p53-independent $p21^{waf1/cip1}$-associated G1 and G2 arrest at higher concentrations that depolymerized microtubules.[37] Based on these in vitro studies, the finding in the present study indicates that the current paclitaxel dosage used for the treatment of prostate cancer may be excessively high, although we should also take into consideration indicators of malignancy, such as the Gleason score, the chemosensitivity of the tumor, and the tumor type.

In summary, gemcitabine intensified the hematological side effects of paclitaxel by pharmacological interaction, but not by pharmacokinetic interaction. In addition, the potency of the hematological side effects in patients treated with gemcitabine was significantly correlated with the paclitaxel exposure. Although the polymorphisms in *MDR1* and *CYP3A5* did not significantly affect the clearance of paclitaxel, monitoring of the serum concentration of paclitaxel might facilitate treatment, with less myelosuppression, without decreasing the therapeutic efficacy of this drug.

Acknowledgments This work was supported in part by a Grant-in-Aid for Scientific Research from the Ministry of Education, Culture, Sports, Science, and Technology of Japan; by a Grant-in-Aid from the Japan Health Science Foundation; and by the Twenty-first Century COE program "Knowledge Information Infrastructure for Genome Science".

References

1. Rowinsky EK (1995) Paclitaxel (Taxol). N Engl J Med 332: 1004–1014
2. Schiff PB, Horwitz SB (1980) Taxol stabilizes microtubules in mouse fibroblast cells. Proc Natl Acad Sci U S A 77:1561–1565
3. Kelly WK, Curley T, Slovin S, et al. (2001) Paclitaxel, estramustine phosphate, and carboplatin in patients with advanced prostate cancer. J Clin Oncol 19:44–53
4. Meluch AA, Greco FA, Burris HA 3rd, et al. (2001) Paclitaxel and gemcitabine chemotherapy for advanced transitional-cell carcinoma of the urothelial tract: a phase II trial of the Minnie Pearl Cancer Research Network. J Clin Oncol 19:3018–3024
5. Gianni L, Kearns CM, Giani A, et al. (1995) Nonlinear pharmacokinetics and metabolism of paclitaxel and its pharmacokinetic/pharmacodynamic relationships in humans. J Clin Oncol 13:180–190
6. Ohtsu T, Sasaki Y, Tamura T, et al. (1995) Clinical pharmacokinetics and pharmacodynamics of paclitaxel: a 3-h infusion versus a 24-h infusion. Clin Cancer Res 1:599–606
7. Huizing MT, Giaccone G, van Warmerdam LJ, et al. (1997) Pharmacokinetics of paclitaxel and carboplatin in a dose-escalating and dose-sequencing study in patients with non-small-cell lung cancer. J Clin Oncol 15:317–329
8. Bruno R, Olivares R, Berille J, et al. (2003) α-1-Acid glycoprotein as an independent predictor for treatment effects and a prognostic factor of survival in patients with non-small cell lung cancer treated with docetaxel. Clin Cancer Res 9:1077–1082
9. Evans WE, McLeod HL (2003) Pharmacogenomics – drug disposition, drug targets, and side effects. N Engl J Med 348:538–549
10. Sonnichen DS, Liu Q, Schuetz EG, et al. (1995) Variability in human cytochrome P450 paclitaxel metabolism. J Pharmacol Exp Ther 275:566–575
11. Sparreboom A, van Asperen J, Mayer U, et al. (1997) Limited oral bioavailability and active epithelial excretion of paclitaxel (Taxol) caused by P-glycoprotein in the intestine. Proc Natl Acad Sci U S A 94:2031–2035
12. Goh BC, Lee SC, Wang LZ, et al. (2002) Explaining interindividual variability of docetaxel pharmacokinetics and pharmacodynamics in Asians through phenotyping and genotyping strategies. J Clin Oncol 20:3683–3690
13. Shou M, Martinet M, Korzekwa KR, et al. (1998) Role of human cytochrome P450 3A4 and 3A5 in the metabolism of taxotere and its derivatives: enzyme specificity, interindividual distribution and metabolic contribution in human liver. Pharmacogenetics 8:391–401
14. Goto M, Masuda S, Kiuchi T, et al. (2004) *CYP3A5**1-carrying graft liver reduces the concentration/oral dose ratio of tacrolimus in recipients of living-donor liver transplantation. Pharmacogenetics 14:471–478
15. Hoffmeyer S, Burk O, van Richter O, et al. (2000) Functional polymorphism of the human multidrug-resistance gene: multiple sequence variations and correlation of one allele with P-glycoprotein expression and activity in vivo. Proc Natl Acad Sci U S A 97:3473–3478
16. Kim RB, Leake BF, Choo EF, et al. (2001) Identification of functionally variant MDR1 alleles among European Americans and African Americans. Clin Pharmacol Ther 70:189–199
17. Goto M, Masuda S, Saito H, et al. (2002) C3435T polymorphism in the MDR1 gene affects the enterocyte expression level of CYP3A4 rather than Pgp in recipients of living-donor liver transplantation. Pharmacogenetics 12:451–457
18. Dai D, Zeldin DC, Blaisdell JA, et al. (2001) Polymorphisms in human CYP2C8 decrease metabolism of the anticancer drug paclitaxel and arachidonic acid. Pharmacogenetics 11:597–607
19. Nakajima M, Fujiki Y, Kyo S, et al. (2005) Pharmacokinetics of paclitaxel in ovarian cancer patients and genetic polymorphisms of CYP2C8, CYP3A4, and MDR1. J Clin Pharmacol 45:674–682
20. Henningsson A, Marsh S, Loos WJ, et al. (2005) Association of CYP2C8, CYP3A4, CYP3A5, and ABCB1 polymorphisms with the pharmacokinetics of paclitaxel. Clin Cancer Res 11:8097–8104
21. Calvert AH, Newell DR, Gumbrell LA, et al. (1989) Carboplatin dosage: prospective evaluation of a simple formula based on renal function. J Clin Oncol 7:1748–1756
22. Jiko M, Yano I, Okuda M, et al. (2005) Altered pharmacokinetics of paclitaxel in experimental hepatic or renal failure. Pharm Res 22:228–234
23. van Schaik RH, de Wildt SN, van Iperen NM, et al. (2000) CYP3A4-V polymorphism detection by PCR-restriction fragment length polymorphism analysis and its allelic frequency among 199 Dutch Caucasians. Clin Chem 46:1834–1836
24. van Schaik RH, de Wildt SN, Brosens R, et al. (2001) The *CYP3A4**3 allele: is it really rare? Clin Chem 47:1104–1106
25. van Schaik RH, vander Heiden IP, van den Anker JN, et al. (2001) CYP3A5 variant allele frequencies in Dutch Caucasians. Clin Chem 48:1668–1671
26. Beal SL, Boeckman AJ, Sheiner LB (1982) NONMEM users guides. NONMEM Project Group, University of California, San Francisco
27. Sonnichsen DS, Hurwitz CA, Pratt CB, et al. (1994) Saturable pharmacokinetics and paclitaxel pharmacodynamics in children with solid tumors. J Clin Oncol 12:532–538
28. Kroep JR, Giaccone G, Voorn DA, et al. (1999) Gemcitabine and paclitaxel: pharmacokinetic and pharmacodynamic interactions in patients with non-small-cell lung cancer. J Clin Oncol 17:2190–2197
29. Dowling TC, Briglia AE, Fink JC, et al. (2003) Characterization of hepatic cytochrome p4503A activity in patients with end-stage renal disease. Clin Pharmacol Ther 73:427–434
30. Kumar GN, Walle UK, Bhalla KN, et al. (1993) Binding of taxol to human plasma, albumin and α_1-acid glycoprotein. Res Commun Chem Pathol Pharmacol 80:337–344
31. Uwai Y, Masuda S, Goto M, et al. (2004) Common single nucleotide polymorphisms of the *MDR1* gene have no influence on its mRNA expression level of normal kidney cortex and renal cell carcinoma in Japanese nephrectomized patients. J Hum Genet 49:40–45
32. Chowbay B, Li H, David M, et al. (2005) Meta-analysis of the influence of MDR1 C3435T polymorphism on digoxin pharmacokinetics and MDR1 gene expression. Br J Clin Pharmacol 60: 159–171
33. Shon JH, Yoon YR, Hong WS, et al. (2005) Effect of itraconazole on the pharmacokinetics and pharmacodynamics of fexofenadine in relation to the genetic polymorphism. Clin Pharmacol Ther 78:191–201
34. Nakajima M, Fujiki Y, Noda K, et al. (2003) Genetic polymorphisms of CYP2C8 in Japanese population. Drug Metab Dispos 31:687–690
35. Torres K, Horwitz SB (1998) Mechanisms of Taxol-induced cell death are concentration dependent. Cancer Res 58:3620–3626
36. Jordan MA, Toso RJ, Thrower D, et al. (1993) Mechanism of mitotic block and inhibition of cell proliferation by taxol at low concentrations. Proc Natl Acad Sci U S A 90:9552–9556
37. Blajeski AL, Phan VA, Kottke TJ, Kaufmann SH (2002) G_1 and G_2 cell-cycle arrest following microtubule depolymerization in human breast cancer cells. J Clin Invest 110:91–99

Am J Physiol Renal Physiol 293: F1564–F1570, 2007.
First published September 12, 2007; doi:10.1152/ajprenal.00322.2007.

Critical roles of Sp1 in gene expression of human and rat H^+/organic cation antiporter MATE1

Moto Kajiwara,[1] Tomohiro Terada,[1] Jun-ichi Asaka,[1] Ken Ogasawara,[1] Toshiya Katsura,[1] Osamu Ogawa,[2] Atsushi Fukatsu,[3] Toshio Doi,[4] and Ken-ichi Inui[1]

[1]Department of Pharmacy, [2]Department of Urology, and [3]Division of Artificial Kidneys, Kyoto University Hospital, Faculty of Medicine, Kyoto University, Kyoto; and [4]Department of Clinical Biology and Medicine, University of Tokushima, Tokushima, Japan

Submitted 13 July 2007; accepted in final form 10 September 2007

Kajiwara M, Terada T, Asaka J, Ogasawara K, Katsura T, Ogawa O, Fukatsu A, Doi T, Inui K. Critical roles of Sp1 in gene expression of human and rat H^+/organic cation antiporter MATE1. *Am J Physiol Renal Physiol* 293: F1564–F1570, 2007. First published September 12, 2007; doi:10.1152/ajprenal.00322.2007.—A H^+/organic cation antiporter (multidrug and toxin extrusion 1: MATE1/SLC47A1) plays important roles in the tubular secretion of various clinically important cationic drugs such as cimetidine. We have recently found that the regulation of this transporter greatly affects the pharmacokinetic properties of cationic drugs in vivo. No information is available about the regulatory mechanisms for the *MATE1* gene. In the present study, therefore, we examined the gene regulation of human (h) and rat (r) MATE1, focusing on basal expression. A deletion analysis suggested that the regions spanning −65/−25 and −146/−38 were essential for the basal transcriptional activity of the hMATE1 and rMATE1 promoter, respectively, and that both regions contained putative Sp1-binding sites. Functional involvement of Sp1 was confirmed by Sp1 overexpression, a mutational analysis of Sp1-binding sites, mithramycin A treatment, and an electrophoretic mobility shift assay. Furthermore, we found a single nucleotide polymorphism (SNP) in the promoter region of *hMATE1* (G−32A), which belongs to a Sp1-binding site. The allelic frequency of this rSNP was 3.7%, and Sp1-binding and promoter activity were significantly decreased. This is the first study to clarify the transcriptional mechanisms of the *MATE1* gene and to identify a SNP affecting the promoter activity of hMATE1.

tubular secretion; basal transcriptional activity; single nucleotide polymorphism; multidrug and toxin extrusion 1

RENAL ELIMINATION, including glomerular filtration and tubular secretion, is a major clearance mechanism for many drugs. The renal tubular secretion of drugs takes place primarily in the proximal tubules as an interplay of drug transporters located in the basolateral and brush-border membranes, respectively. For example, organic cations are taken up by membrane potential-dependent organic cation transporters and then extruded into the lumen by H^+/organic cation antiporters (14). Molecular cloning of membrane potential-dependent organic cation transporter 1 (OCT1) was reported in 1994 (12), and at present, three kinds of organic cation transporters (OCT1–3) from various species have been identified and characterized (7, 14, 36). In contrast to OCTs, attempts at the molecular identification of apical H^+/organic cation antiporters have failed for more than a decade.

Recently, mammalian orthologs of the multidrug and toxin extrusion (MATE) family, which confers multidrug resistance on bacteria, have been identified in humans (19, 25), mice (25), rats (23, 34), and rabbits (37). Two functional isoforms, MATE1/SLC47A1 (human, mouse, rat, and rabbit) and MATE2-K/SLC47A2 (human and rabbit), have been characterized in terms of tissue distribution, membrane localization, and transport characteristic and have been demonstrated to work as H^+/organic cation antiporters (2, 19, 20, 23, 25, 33–35, 37). MATE1 is able to transport various organic cations such as tetraethylammonium, cimetidine, and metformin and the zwitterion cephalexin using an oppositely directed H^+ gradient (33–35). Human (h) MATE1 is primarily expressed in the kidney and liver and is located at the membranes of the luminal side (19, 25). Rat (r) MATE1 is also present in the brush-border membranes of renal proximal tubules (20), and the intrarenal expression of rMATE1 is limited to the proximal tubules (34). Our group (20) also demonstrated that the expression level of rMATE1 was remarkably reduced in 5/6 nephrectomized rats and that the level of rMATE1, but not of rOCT2, correlated well with the tubular secretion of cimetidine in female rats ($r = 0.74$). Furthermore, very recently, our group identified cysteine and histidine residues essential to the function of rat and human MATE1 (2). Hence, functional and expressional aspects of MATE1 have been clarified in much detail, but there has been no information about the transcriptional regulation including basal promoter activity of this transporter.

The core promoter and proximal promoter regions contain elements that control the initiation of transcription, and therefore, essential regions that harbor functionally relevant polymorphisms may have significant effects on gene expression (6). When such polymorphisms occur in the promoter region of pharmacokinetic-related genes, drug disposition, efficacy, and toxicity can be influenced. For example, a genetic polymorphism of the uridine diphosphate-glucuronosyltransferase 1A1 gene, *UGT1A1*28*, a variant sequence in the promoter region, contributed to individual variation for adverse events in patients administered the anti-cancer agent irinotecan (13). Thus a search for single nucleotide polymorphisms in the promoter region (rSNP) of drug transporters may provide useful information on interindividual differences in drug disposition.

In the present study, therefore, we characterized the promoter activity of hMATE1 and rMATE1 to identify the min-

Address for reprint requests and other correspondence: Prof. K. Inui, Dept. of Pharmacy, Kyoto Univ. Hospital, Sakyo-ku, Kyoto 606-8507, Japan (e-mail: inui@kuhp.kyoto-u.ac.jp).

The costs of publication of this article were defrayed in part by the payment of page charges. The article must therefore be hereby marked "*advertisement*" in accordance with 18 U.S.C. Section 1734 solely to indicate this fact.

imal region and *cis*-regulatory elements required for the basal expression of *MATE1*. Furthermore, we performed rSNP analyses for *hMATE1* and found that SNP at G−32A, which belongs to a Sp1-binding site, affected the promoter activity of the gene.

MATERIALS AND METHODS

Materials. [γ-^{32}P]ATP was obtained from GE Healthcare (Little Chalfont, UK). Restriction enzymes were obtained from New England BioLabs (Beverly, MA). Antibody for Sp1 (H-225) was purchased from Santa Cruz Biotechnology (Santa Cruz, CA). Mithramycin A was purchased from Sigma-Aldrich (St. Louis, MO). The plasmid CMV-Sp1 was kindly provided by Dr. Robert Tjian (University of California, Berkeley, CA). All other chemicals used were of the highest purity available.

Determination of putative transcriptional start site. To identify the transcription start site of hMATE1 and rMATE1, we carried out 5′-rapid amplification of cDNA ends (5′-RACE) using human and rat kidney Marathon-Ready cDNA (Clontech, Mountain View, CA), respectively, according to the manufacturer's instructions. The primers for 5′-RACE were as follows: a gene-specific primer for hMATE1 (GenBank accession no. FLJ10847), 5′-CAGGACCAAGAGCGCCCGCAGCTCTTCT-3′ (209/182); a nested gene-specific primer for hMATE1, 5′-CTGGCGCGGGCTCCTCAGGAGCTTCCAT-3′ (114/87); a gene-specific primer for rMATE1 (GenBank accession no. NM_001014118), 5′-GAGCTGGGCCAAGAACGCAGGACCC-3′ (170/146); and a nested gene-specific primer for rMATE1, 5′-CTGGTCCCGGCGCAGGCTCCTCCAAGA-3′ (57/31). The polymerase chain reaction (PCR) products were subcloned into the pGEM-T Easy Vector (Promega, Madison, WI). All PCR products were sequenced using a multicapillary DNA sequencer RISA384 system (Shimadzu, Kyoto, Japan).

Construction of reporter plasmids for hMATE1 and rMATE1 promoters. The human or rat promoter region upstream of the transcription start site was amplified by PCR using human genomic DNA (Promega) or rat genomic DNA (Clontech) with the primers listed in Table 1. The PCR products were subcloned into the firefly luciferase reporter vector pGL3-Basic (Promega). The full-length reporter plasmids are hereafter referred to as hMATE1 (−2408/+13) and rMATE1 (−2422/+24). The 5′-deleted constructs were generated by digestion with appropriate restriction enzymes. The hMATE1 (−65/+13) and rMATE1 (−38/+24) constructs were generated by PCR with the primers listed in Table 1. The site-directed mutations in putative Sp1-binding sites were introduced into the hMATE1 (−65/+13) construct with a QuickChange II site-directed mutagenesis kit (Stratagene, La Jolla, CA) with the primers listed in Table 1. All PCR products and deletion constructs for reporter assays or rSNP analyses were sequenced using a multicapillary DNA sequencer RISA384 system (Shimadzu).

Cell culture, transfection, and reporter gene assays. LLC-PK$_1$ and HEK293 cells were obtained from the American Type Culture Collection (ATCC CRL-1392 and -1573). Cell culture, transfection, and reporter gene assays were carried out as described previously (1, 22, 29).

Western blot analysis. Preparation of nuclear extracts from LLC-PK$_1$ cells was described previously (29). The nuclear extracts of LLC-PK$_1$ cells (125 ng) were solubilized in SDS sample buffer, separated on a 10% polyacrylamide gel, and transferred onto polyvinylidene difluoride membranes (Immobilon-P; Millipore, Bedford, MA) by semidry electroblotting. Blots were blocked with 5% nonfat dry milk in Tris-buffered saline (TBS; 20 mM Tris, 137 mM NaCl, pH 7.5) with 0.1% Tween 20 (TBS-T) for 1 h at room temperature. Blots were washed in TBS-T and then incubated with the anti-Sp1 polyclonal antibody (1 μg/ml, overnight at 4°C). The bound antibody was detected on X-ray film by enhanced chemiluminescence with a horse-

Table 1. *Primer sequences*

Reporter Construct	Direction	Sequence (5′-3′)	Position
hMATE1	Forward	GGACGCGTCAGCCAACCACACGTTGTTTTA	−2408/−2387
(−2408/+13)	Reverse	GGAAGCTTGGAGGCCGGCAGTGAGTACC	+13/−7
rMATE1	Forward	GGACGCGTTCTTGGTGGGGGAACCCCAGT	−2522/−2502
(−2422/+24)	Reverse	GGAGATCTGTGGCCTCCGTGCTGTCGGG	+24/+4
hMATE1	Forward	GGACGCGTCGGGGCGGGCTCTGGGC	−65/−49
(−65/+13)	Reverse	GGAAGCTTGGAGGCCGGCAGTGAGTACC	+13/−7
rMATE1	Forward	GGACGCGTTTCAGGCCTGTGGGTCC	−38/−21
(−38/+24)	Reverse	GGAGATCTGTGGCCTCCGTGCTGTCGGG	+24/+4
		Site-directed mutagenesis for hMATE1 reporter construct	
Mutation A	Forward	GGGCGCCAGGCGCGGAACGTGCTCTGGGCG	−77/−48
	Reverse	CGCCCAGAGCACGTTCCGCGCCTGGCGCCC	−48/−77
Mutation B	Forward	GGGCGGCCGGAACGTGGACTGCAGAGCAGGC	−48/−18
	Reverse	GCCTGCTCTGCAGTCCACGTTCCGGCCGCCC	−18/−48
SNP	Forward	GCGGGCGGCCGGGGCGGGAACTGCAGAGC	−50/−22
	Reverse	GCTCTGCAGTTCCCGCCCCGGCCGCCCGC	−22/−50
		Oligonucleotides for hMATE1 EMSA	
Wild *probe A*	Forward	GGGCGCCAGGCGCGGGGCGGGCTCTGGGCG	−77/−48
	Reverse	CGCCCAGAGCCCGCCCCGCGCCTGGCGCCC	−48/−77
Wild *probe B*	Forward	GGGCGGCCGGGGCGGGGACTGCAGAGCAGGC	−48/−18
	Reverse	GCCTGCTCTGCAGTCCCCGCCCCGGCCGCCC	−18/−48
Mutational *probe A*	Forward	GGGCGCCAGGCGCGGAACGTGCTCTGGGCG	−77/−48
	Reverse	CGCCCAGAGCACGTTCCGCGCCTGGCGCCC	−48/−77
Mutational *probe B*	Forward	GGGCGGCCGGAACGTGGACTGCAGAGCAGGC	−48/−18
	Reverse	GCCTGCTCTGCAGTCCACGTTCCGGCCGCCC	−18/−48
SNP *probe B*	Forward	GGGCGGCCGGGGCGGGAACTGCAGAGCAGGC	−48/−18
	Reverse	GCCTGCTCTGCAGTTCCCGCCCCGGCCGCCC	−18/−48

Primer sequences are shown for human (h) and rat (r) multidrug and toxin extrusion 1 (MATE1) constructs. *Mlu*I, *Hin*dIII, and *Bgl*II sites are underlined. Mutations introduced into the oligonucleotides are shown in bold. SNP, single nucleotide polymorphism.

radish peroxidase-conjugated anti-rabbit IgG antibody (GE Healthcare).

EMSA. Recombinant human Sp1 (rhSp1) and recombinant human Sp3 (rhSp3) were obtained from Promega and Alexis (Lausen, Switzerland), respectively. The probes shown in Table 1 were prepared by annealing complementary sense and antisense oligonucleotides, followed by end labeling with [γ-^{32}P]ATP using T4 polynucleotide kinase (Takara Bio, Otsu, Japan) and purification through a Sephadex G-25 column (GE Healthcare). The composition of the binding mixture containing rhSp1 was based on Martín et al. (17), and compositions of rhSp3 binding buffer were as follows: 1 mM $MgCl_2$, 0.5 mM EDTA, 0.5 mM DTT, 50 mM NaCl, 10 mM Tris·HCl (pH 7.5), and 4% glycerol. Labeled probes were added to the binding mixture and incubated for 0.5–1 h at room temperature. The DNA-protein complexes were then separated on a 4% polyacrylamide gel at room temperature in 0.5× Tris-borate-EDTA buffer. The gel was dried and exposed to X-ray film for autoradiography.

rSNP analyses. Genomic DNA was extracted from peripheral blood from 88 patients with renal diseases (47 men and 41 women; range 14–78 yr) and normal parts of the kidney from 21 renal cell carcinoma patients (21 men; range 39–77 yr) using a Wizard Genomic DNA purification kit (Promega). About 120 bp of the promoter region of the *hMATE1* gene were amplified by PCR using

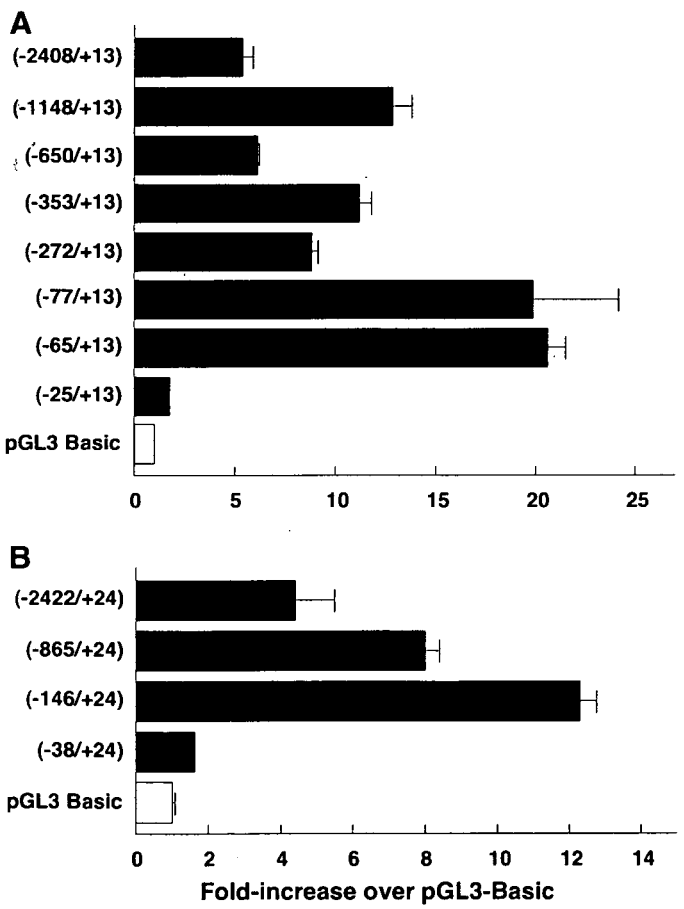

Fig. 1. Deletion analysis of human multidrug and toxin extrusion 1 (hMATE1) and rat (r)MATE1 promoter activity in LLC-PK_1 cells. *A*: a series of hMATE1 deleted promoter constructs (equimolar amounts of the −2408/+13 construct; 600 ng) were transfected into LLC-PK_1 cells for luciferase assays. *B*: a series of rMATE1 deleted promoter constructs (equimolar amounts of the −2422/+24 construct; 600 ng) were transfected into LLC-PK_1 cells for luciferase assays. Firefly luciferase activity was normalized to *Renilla* luciferase activity. Data are reported as the relative increase compared with pGL3-Basic and are means ± SE of 3 replicates.

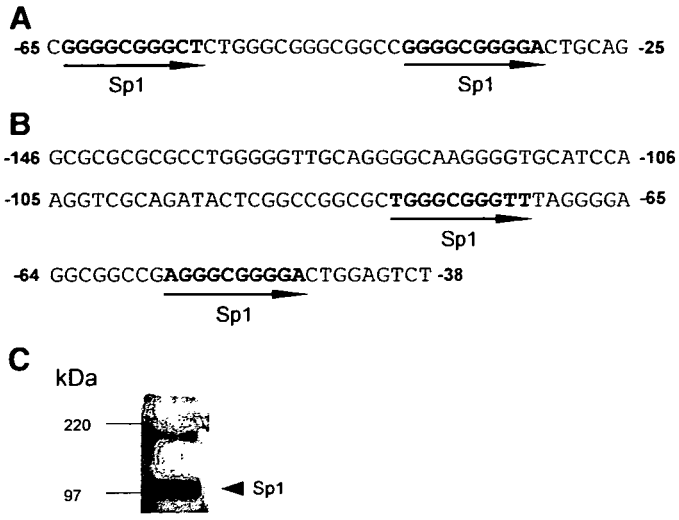

Fig. 2. Nucleotides sequence of the hMATE1 (*A*) and rMATE1 (*B*) promoter. Numbering is relative to the transcription start site. The putative binding sites for Sp1 are indicated on the sequence (arrows indicate the direction). *C*: detection of Sp1 by Western blot analysis. Nuclear extracts from LLC-PK_1 cells (125 ng) were separated on a 10% SDS-polyacrylamide gel and blotted onto a polyvinylidene difluoride membrane. Sp1 antibody (1 μg/ml) was used as a primary antibody. Horseradish peroxidase-conjugated anti-rabbit IgG antibody was used for detection of bound antibody. The arrowhead indicates the position of Sp1.

the forward primer 5′-CGCAGTGGTGCAGAGAGAGGTGCAA-3′ (−154/−130) and the reverse primer 5′-AGTCACCCGCGGAGGCAGAAATCAC-3′ (297/273). PCR conditions were as follows: denaturation at 94°C for 30 s, annealing and synthesis at 68°C for 3 min, for 35 cycles. All PCR products were sequenced using a multicapillary DNA sequencer RISA384 system (Shimadzu).

This study was conducted in accordance with the Declaration of Helsinki and its amendments and was approved by the Kyoto University Graduate School and Faculty of Medicine Ethics Committee.

Data analysis. The results are mainly expressed relative to pGL3-Basic and represent means ± SE of three replicates. Two or three experiments were conducted, and representative results are shown. Data were analyzed statistically with one-way ANOVA followed by Dunnett's test.

RESULTS

Determination of the transcription start site of hMATE1 and rMATE1. Sequencing of the longest RACE product showed that the terminal position of hMATE1 and rMATE1 cDNA was located 22 and 20 nucleotides upstream of the start codon, which was 64 and 3 bp downstream of the 5′-end of hMATE1 and rMATE1 cDNA, respectively, registered in the National Center for Biotechnology Information database [GenBank accession no. FLJ10847 (hMATE1) and NM_001014118 (rMATE1)]. Therefore, the 5′-end of hMATE1 and rMATE1 cDNA in the database was numbered with +1 as the transcription start site in this study.

Determination of the minimal hMATE1 and rMATE1 promoter. To determine the minimal region required for basal activity of the promoter, a series of hMATE1 (Fig. 1*A*) or rMATE1 (Fig. 1*B*) deletion constructs were transfected into LLC-PK_1 cells, and luciferase activity was measured. In LLC-PK_1 cells, the H^+/organic cation antiport system is expressed in the apical membrane (9, 15, 28), and we hypothesized that transcription factors and/or cofactors required for the expres-

sion of MATE1 exist intrinsically in these cells. The longest reporter constructs of hMATE1 and rMATE1 showed an approximately three- to fivefold increase in luciferase activity compared with pGL3-Basic. The luciferase activity of both constructs was completely abolished with the −25/+13 (hMATE1) and −38/+24 (rMATE1) deleted promoter constructs, respectively, suggesting that the region between −65 and −25 for hMATE1 or between −146 and −38 for rMATE1 was important for basal promoter activity. We then performed a computational sequence analysis of these regions using TFSEARCH (www.cbrc.jp/research/db/TFSEARCH.html). This analysis revealed that the region proximal to the transcription start site lacks canonical TATA or CCAAT boxes. Instead, two GC-rich sites were observed, suggesting a possible contribution of Sp1 to the basal promoter activity of MATE1 (Fig. 2, *A* and *B*).

Western blot analysis. To confirm the expression of Sp1 in LLC-PK$_1$ cells, we carried out Western blot analysis for Sp1. As shown in Fig. 2*C*, an immunoreactive protein with a molecular mass of 106 kDa corresponding to Sp1 was detected in LLC-PK$_1$ cells.

Functional involvement of Sp1 in MATE1 promoter activity. To evaluate the functional involvement of Sp1 in MATE1 promoter activity, we performed experiments for the inhibition and transactivation of Sp1. Mithramycin A is known to bind to the GC box and inhibit Sp1 binding (4, 27). As shown in Fig. 3, treatment with mithramycin A led to a significant decrease in the promoter activity in a dose-dependent manner for both reporter constructs. Next, we investigated the effect of Sp1 overexpression on the MATE1 promoter activity in HEK293 cells (Fig. 4). Transfection of the CMV-Sp1 expression vector in LLC-PK$_1$ cells remarkably reduced the activity of the pGL3-Basic (control) via unknown mechanisms, and therefore, HEK293 cells were used for Sp1 overexpression experiments. The promoter activity of hMATE1 (−65/+13) or rMATE1 (−146/+24) showed a dose-dependent increase in the cotransfection of CMV-Sp1, providing direct evidence that Sp1 enhanced the activity.

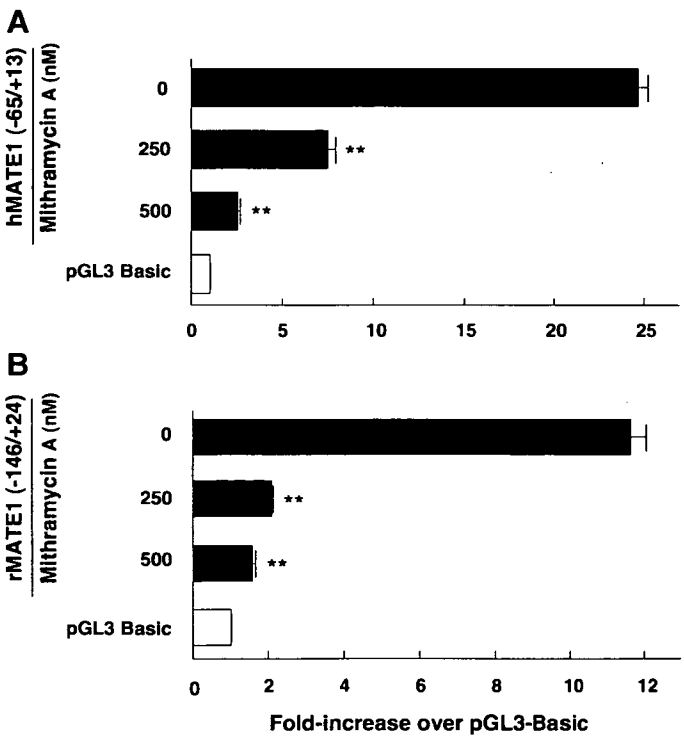

Fig. 3. Inhibition of hMATE1 (*A*) and rMATE1 (*B*) transcriptional activity by mithramycin A. LLC-PK$_1$ cells were transiently transfected with the hMATE1 (−65/+13) or rMATE1 (−146/+24) construct (same amount as in the deletion analysis). Mithramycin A was added to the cells 5 h after the transfection. Firefly luciferase activity was normalized to *Renilla* luciferase activity. Data are reported as the relative increase compared with pGL3-Basic and are means ± SE of 3 replicates. $^{**}P < 0.01$, significantly different from the values without mithramycin A.

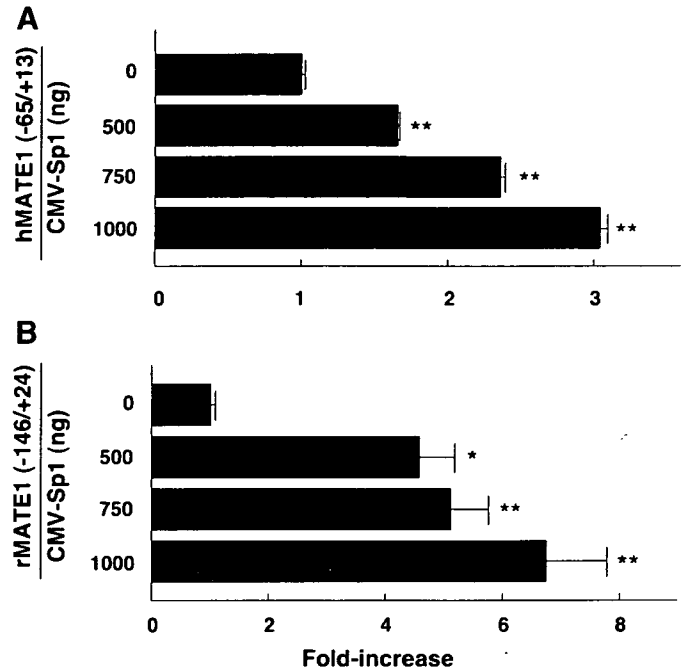

Fig. 4. Effect of Sp1 overexpression on hMATE1 (*A*) and rMATE1 (*B*) transcriptional activity. HEK293 cells were transiently transfected with 250 ng of hMATE1 (−65/+13) or rMATE1 (−146/+24) construct with the CMV-Sp1 expression vector (500, 750, and 1,000 ng). The total amount of transfected DNA was kept constant by adding empty vector. Data are reported as the relative increase compared with that without CMV-Sp1 and are means ± SE of 3 replicates. $^{*}P < 0.05$; $^{**}P < 0.01$, significantly different from the values without CMV-Sp1.

Identification of Sp1-binding site of hMATE1 promoter. In the proximal hMATE1 promoter region, there are two putative Sp1-binding sites located between −65 and −25, and these sites were designated as Sp-A (−64/−55) and Sp-B (−40/−31), respectively. To determine whether these sites were important for hMATE1 promoter activity, we introduced a mutation at each site of the hMATE1 (−65/+13) construct (*mutation A* and *mutation B*; Fig. 5*A*). As shown in Fig. 5*B*, both mutants remarkably reduced the luciferase activity compared with the wild type. These results suggest that both Sp-A and Sp-B are important for regulating the hMATE1 promoter activity. Finally, to confirm that Sp1 binds to Sp-A and Sp-B sites, we performed EMSAs with rhSp1 and wild-type or mutational probes of Sp-A and Sp-B (Fig. 5*A*). Both *wild probes A* and *B* formed DNA-protein complexes (Fig. 6*A*, *lanes 3* and *7*), whereas no complex was formed in the absence of rhSp1 or *mutational probes A*

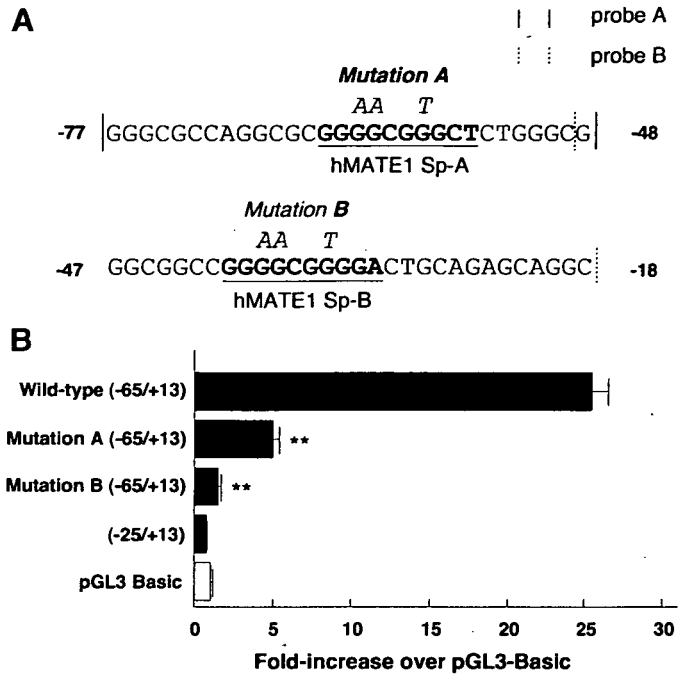

Fig. 5. Mutational analysis of the putative Sp1-binding sites of the hMATE1 promoter. *A*: the nucleotide sequence of the promoter region from −77 to −18 is shown with the putative Sp1-binding elements (Sp-A and Sp-B underlined). Site-directed mutations that destroy Sp1-binding elements were introduced individually and designated *mutation A* and *mutation B*. The nucleotides altered for mutational analysis are shown italicized above the wild-type sequence. The regions used for oligonucleotide probes for EMSA are also indicated. *B*: the mutated −65/+13 constructs (same amount as in the deletion analysis) were transiently expressed in LLC-PK$_1$ cells for luciferase assays. Firefly luciferase activity was normalized to *Renilla* luciferase activity. Data are reported as the relative increase compared with pGL3-Basic and are means ± SE of 3 replicates. $^{**}P < 0.01$, significantly different from the wild type.

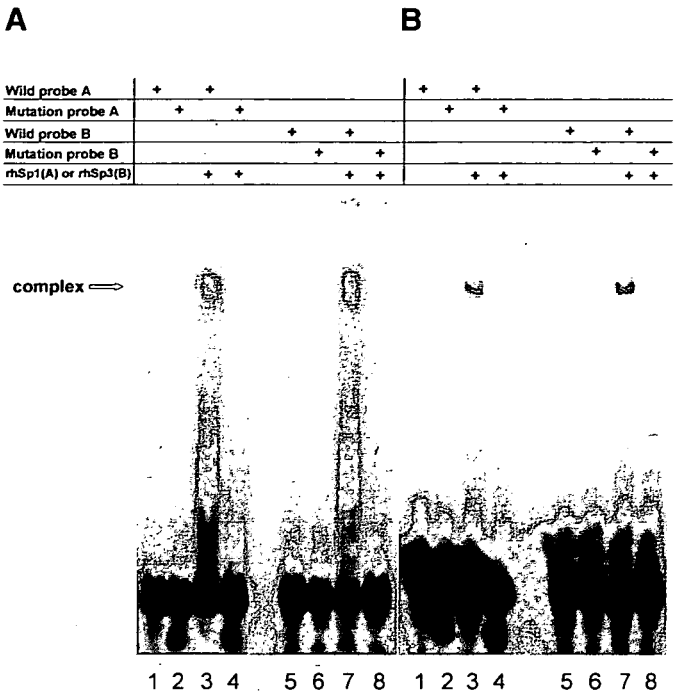

Fig. 6. EMSA of recombinant human (rh)Sp1 (*A*) or rhSp3 (*B*) proteins binding to the hMATE1 probes containing putative Sp1-binding elements. rhSp1 (30 ng) or rhSp3 (10 ng) was incubated with the wild or mutated [γ-^{32}P]ATP-labeled oligonucleotide probes [*probe A* (−77/−48) and *probe B* (−48/−18)] in *lanes 3*, *4*, *7*, and *8*. In *lanes 1*, *2*, *5*, and *6*, rhSp1 (*A*) or rhSp3 (*B*) was not added.

and *B* (Fig. 6*A*, *lanes 1*, *2*, *4–6*, and *8*). These results suggest that Sp1 stimulates the basal promoter activity of hMATE1 via Sp-A and Sp-B regions. It was reported that Sp3 as well as Sp1 also recognizes classic Sp1-binding sites (5). We then further examined the interaction of Sp-A and Sp-B with rhSp3. As observed in rhSp1, specific DNA-protein complexes in both *wild probes A* and *B* were detected (Fig. 6*B*).

rSNP Analyses of hMATE1. We then sequenced the promoter region (~120 bp) of the *MATE1* gene in 88 patients with renal diseases and 21 patients with renal cell carcinoma and found the G−32A SNP at the Sp-B site. The frequency of this rSNP is summarized in Table 2. To evaluate the effect of the G−32A SNP on the promoter activity of hMATE1, we carried out an EMSA and a reporter assay. Both wild and SNP probes formed DNA-protein complexes, although less complex was formed with the SNP probe (−32A) (Fig. 7, *lanes 4* and *8*) than with the wild probe (−32G) (Fig. 7, *lanes 3* and *7*). No complex was formed in the absence of rhSp1 (Fig. 7, *lanes 1*, *2*, *5*, and *6*). Furthermore, as shown in Fig. 8, the SNP construct (−32A) remarkably reduced the luciferase activity compared with the wild type (−32G). These results indicate that the G−32A substitution downregulates the basal promoter activity of hMATE1 by weakening the binding of Sp1.

DISCUSSION

In the present study, we performed a functional promoter assay of human and rat *MATE1* genes and obtained convincing evidence of the involvement of Sp1 in the regulation of the basal expression of these transporters. This conclusion is supported by results of experiments involving the inhibition of mithramycin A, the overexpression of Sp1, mutagenesis of the GC-rich region, and EMSAs using rhSp1. In the proximal promoter region of the human and rat *MATE1* genes, two GC-rich sites exist instead of a TATA box, and these features are conserved among species (Fig. 9). In a TATA-less promoter, Sp1 binds to the GC-rich region to recruit TATA-binding protein (26) and to fix the transcription start site (3). Furthermore, it was reported that the promoter activity is enhanced if multiple Sp1-binding sites exist (18). These findings suggested that Sp1 plays a significant role as a basal transcription factor through these GC-rich sites in the MATE1 promoter.

Furthermore, we found a SNP at a Sp1-binding site (G−32A, belonging to the Sp-B site) of the hMATE1 promoter for the first time and demonstrated that this substitution affects hMATE1 promoter activity by disrupting the binding of Sp1. It

Table 2. *Allelic frequency of G−32A of hMATE1 for 109 patients with renal diseases and renal cell carcinoma*

Gene	Location	Genotype	*n*	Frequency, %
hMATE1	−32	G/G	105	96.3
		G/A	4	3.7

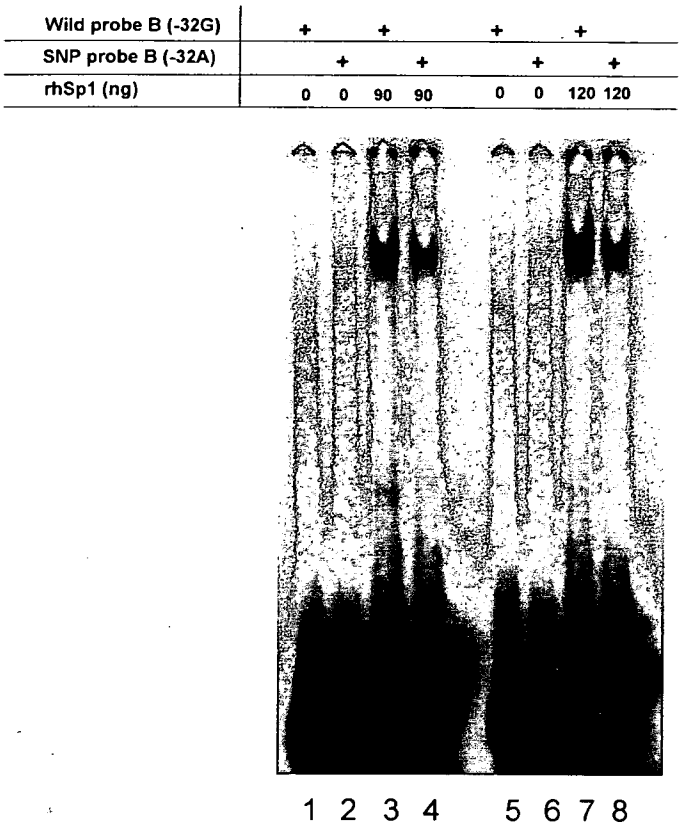

Fig. 7. Effect of single nucleotide polymorphism (SNP; G−32A) on EMSA for rhSp1. rhSp1 (90 or 120 ng) was incubated with the wild probe (−32G) in *lanes 3* and *4*) or the SNP probe (−32A) in *lanes 7* and *8*. In *lanes 1*, *2*, *5*, and *6*, rhSp1 was not added.

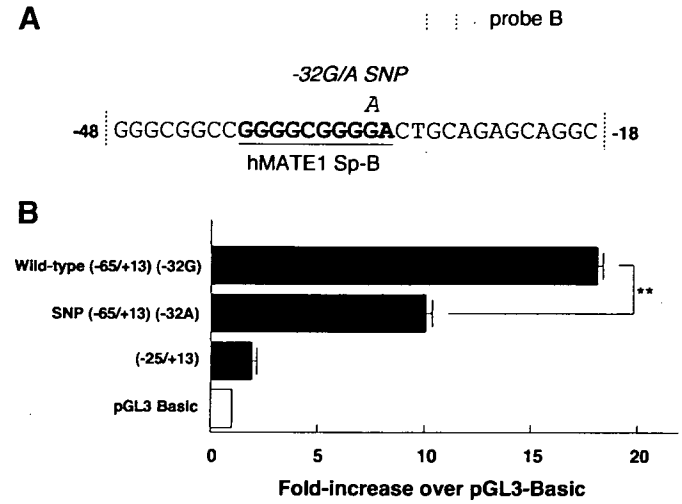

Fig. 8. Effect of rSNP (G−32A) of the putative Sp1-binding sites on the hMATE1 promoter activity. *A*: the nucleotide sequence of the promoter region from −48 to −18 is shown. *B*: the SNP −65/+13 constructs were transiently expressed in LLC-PK_1 cells for luciferase assays. Firefly luciferase activity was normalized to *Renilla* luciferase activity. Data are reported as the relative increase compared with pGL3-Basic and are means ± SE of 3 replicates. $^{**}P < 0.01$, significantly different from the wild type.

is strongly suggested that this rSNP influences the mRNA level of MATE1.

To date, many large-scale screenings of SNPs of drug transporters (mainly focusing on SNPs in the coding region; cSNPs) have been carried out to identify genetic factors involved in the interindividual differences of pharmacokinetics. So far, clinical implications for cSNPs in the genes for organic anion transporting polypeptides (16) and OCT1 (31, 32) have been demonstrated, but significant results have not been obtained for other SLC-type drug transporters. In the present study, we found an rSNP of Sp1-binding sites affecting the *MATE1* gene. This type of SNP may be involved in the interindividual differences of pharmacokinetics. There are reports that rSNPs of Sp1-binding sites of the resistin gene contribute to type 2 diabetes mellitus susceptibility (24) and that those of the collagen type I α1 gene contribute to low bone mass and vertebral fracture (11). Further studies of the relationship between gene polymorphisms of *MATE1* and the pharmacokinetic properties of MATE1 substrate drugs may clarify the clinical implications of this SNP.

Human and rat MATE1 mRNA is abundantly expressed in the kidney (19, 34), whereas Sp1 is expressed ubiquitously. The present study revealed the contribution of Sp1 to the transcriptional regulation of MATE1, but the mechanism of this tissue-specific expression has not been clarified. In the case of intestinal H^+-coupled peptide transporter 1, the basal promoter activity was also determined by Sp1, but its tissue specific expression was regulated by the intestinal specific transcription factor Cdx2 (29, 30). Currently, there is little information about the renal specific transcription factor. It has been reported that Sp3 as well as Sp1 also recognizes classic Sp1-binding sites, and there are a number of reports that the relative abundance of Sp1 and Sp3 should allow regulation of gene activities (5). We confirmed by EMSA that a recombinant Sp3 protein bound to the Sp-A and Sp-B sites of the hMATE1 promoter (Fig. 6*B*). Another possible mechanism is the methylation of the GC box in the promoter region. Methylation of the cytosine residue in the sequence of 5′-CpG-3′ is an epigenetic modification, and recent reports have revealed that this epigenetic modification contributes to the tissue-specific expression (8, 10, 21). Further studies are needed to clarify the tissue-specific expression of MATE1.

In conclusion, the present study clearly indicates that Sp1 functions as a basal transcriptional regulator of the human and rat *MATE1* gene through the two GC boxes, and this system may be conserved among species. Furthermore, we have identified an rSNP of the *hMATE1* gene (G−32A) (belonging to a Sp1-binding site) that affects the promoter activity.

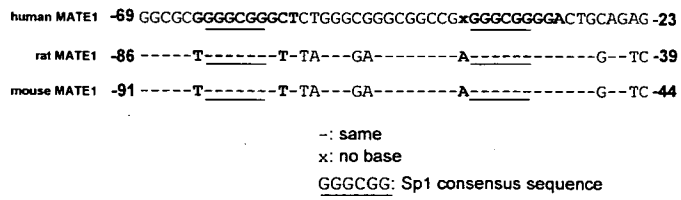

Fig. 9. Nucleotide sequences of the human, rat, and mouse MATE1 promoter. The nucleotide sequences of the promoter region of the human (−69/−23), rat (−86/−39), and mouse (−91/−44) MATE1 are shown with the putative Sp1-binding elements. All of the promoter sequences have the Sp1 consensus sequence (GGGCGG). The putative Sp1-binding sites are shown in bold.

ACKNOWLEDGMENTS

We are grateful to Dr. Robert Tjian (University of California, Berkeley) for the Sp1 expression vector.

GRANTS

This work was supported by the 21st Century Center of Excellence Program "Knowledge Information Infrastructure for Genome Science," a Grant-in-Aid for Scientific Research from the Ministry of Education, Culture, Sports, Science and Technology of Japan, and a Grant-in-Aid for Research on Advanced Medical Technology from the Ministry of Health, Labor and Welfare of Japan.

REFERENCES

1. **Asaka J, Terada T, Okuda M, Katsura T, Inui K.** Androgen receptor is responsible for rat organic cation transporter 2 gene regulation but not for rOCT1 and rOCT3. *Pharm Res* 23: 697–704, 2006.
2. **Asaka J, Terada T, Tsuda M, Katsura T, Inui K.** Identification of essential histidine and cysteine residues of H^+/organic cation antiporter, multidrug and toxin extrusion (MATE). *Mol Pharmacol* 46: 1487–1493, 2007.
3. **Blake MC, Jambou RC, Swick AG, Kahn JW, Azizkhan JC.** Transcriptional initiation is controlled by upstream GC-box interactions in a TATAA-less promoter. *Mol Cell Biol* 10: 6632–6641, 1990.
4. **Blume SW, Snyder RC, Ray R, Thomas S, Koller CA, Miller DM.** Mithramycin inhibits SP1 binding and selectively inhibits transcriptional activity of the dihydrofolate reductase gene in vitro and in vivo. *J Clin Invest* 88: 1613–1621, 1991.
5. **Bouwman P, Philipsen S.** Regulation of the activity of Sp1-related transcription factors. *Mol Cell Endocrinol* 195: 27–38, 2002.
6. **Buckland PR.** The importance and identification of regulatory polymorphisms and their mechanisms of action. *Biochim Biophys Acta* 1762: 17–28, 2006.
7. **Burckhardt G, Wolff NA.** Structure of renal organic anion and cation transporters. *Am J Physiol Renal Physiol* 278: F853–F866, 2000.
8. **Douet V, Heller MB, Le Saux O.** DNA methylation and Sp1 binding determine the tissue-specific transcriptional activity of the mouse *Abcc6* promoter. *Biochem Biophys Res Commun* 354: 66–71, 2007.
9. **Fouda AK, Fauth C, Roch-Ramel F.** Transport of organic cations by kidney epithelial cell line LLC-PK_1. *J Pharmacol Exp Ther* 252: 286–292, 1990.
10. **Fujii G, Nakamura Y, Tsukamoto D, Ito M, Shiba T, Takamatsu N.** CpG methylation at the USF-binding site is important for the liver-specific transcription of the chipmunk *HP-27* gene. *Biochem J* 395: 203–209, 2006.
11. **Grant SFA, Reid DM, Blake G, Herd R, Fogelman I, Ralston SH.** Reduced bone density and osteoporosis associated with a polymorphic Sp1 binding site in the collagen type I α1 gene. *Nat Genet* 14: 203–205, 1996.
12. **Gründemann D, Gorboulev V, Gambaryan S, Veyhl M, Koepsell H.** Drug excretion mediated by a new prototype of polyspecific transporter. *Nature* 372: 549–552, 1994.
13. **Hasegawa Y, Ando Y, Ando M, Hashimoto N, Imaizumi K, Shimokata K.** Pharmacogenetic approach for cancer treatment-tailored medicine in practice. *Ann NY Acad Sci* 1086: 223–232, 2006.
14. **Inui K, Masuda S, Saito H.** Cellular and molecular aspects of drug transport in the kidney. *Kidney Int* 58: 944–958, 2000.
15. **Inui K, Saito H, Hori R.** H^+-gradient-dependent active transporter of tetraethylammonium cation in apical-membrane vesicles isolated from kidney epithelial cell line LLC-PK_1. *Biochem J* 227: 199–203, 1985.
16. **Maeda K, Ieiri I, Yasuda K, Fujino A, Fujiwara H, Otsubo K, Hirano M, Watanabe T, Kitamura Y, Kusuhara H, Sugiyama Y.** Effects of organic anion transporting polypeptide 1B1 haplotype on pharmacokinetics of pravastatin, valsartan, and temocapril. *Clin Pharmacol Ther* 79: 427–439, 2006.
17. **Martín MG, Wang J, Solorzano-Vargas RS, Lam JT, Turk E, Wright EM.** Regulation of the human Na^+-glucose cotransporter gene, *SGLT1*, by HNF-1 and Sp1. *Am J Physiol Gastrointest Liver Physiol* 278: G591–G603, 2000.
18. **Mastrangelo IA, Courey AJ, Wall JS, Jackson SP, Hough PVC.** DNA looping and Sp1 multimer links: a mechanism for transcriptional synergism and enhancement. *Proc Natl Acad Sci USA* 88: 5670–5674, 1991.
19. **Masuda S, Terada T, Yonezawa A, Tanihara Y, Kishimoto K, Katsura T, Ogawa O, Inui K.** Identification and functional characterization of a new human kidney-specific H^+/organic cation antiporter, kidney-specific multidrug and toxin extrusion 2. *J Am Soc Nephrol* 17: 2127–2135, 2006.
20. **Nishihara K, Masuda S, Ji L, Katsura T, Inui K.** Pharmacokinetic significance of luminal multidrug and toxin extrusion 1 in chronic renal failure rats. *Biochem Pharmacol* 73: 1482–1490, 2007.
21. **Nomura J, Hisatsune A, Miyata T, Isohoma Y.** The role of CpG methylation in cell type-specific expression of the aquaporin-5 gene. *Biochem Biophys Res Commun* 353: 1017–1022, 2007.
22. **Ogasawara K, Terada T, Asaka J, Katsura T, Inui K.** Hepatocyte nuclear factor-4α regulates the human organic anion transporter 1 gene in the kidney. *Am J Physiol Renal Physiol* 292: F1819–F1826, 2007.
23. **Ohta K, Inoue K, Hayashi Y, Yuasa H.** Molecular identification and functional characterization of rat multidrug and toxin extrusion type transporter 1 as an organic cation/H^+ antiporter in the kidney. *Drug Metab Dispos* 34: 1868–1874, 2006.
24. **Osawa H, Yamada K, Onuma H, Murakami A, Ochi M, Kawata H, Nishimiya T, Niiya T, Shimizu I, Nishida W, Hashiramoto M, Kanatsuka A, Fujii Y, Ohashi J, Makino H.** The G/G genotype of a resistin single-nucleotide polymorphism at −420 increases type 2 diabetes mellitus susceptibility by inducing promoter activity through specific binding of Sp1/3. *Am J Hum Genet* 75: 678–686, 2004.
25. **Otsuka M, Matsumoto T, Morimoto R, Arioka S, Omote H, Moriyama Y.** A human transporter protein that mediates the final excretion step for toxic organic cations. *Proc Natl Acad Sci USA* 102: 17923–17928, 2005.
26. **Pugh BF, Tjian R.** Transcription from a TATA-less promoter requires a multisubunit TFIID complex. *Genes Dev* 5: 1935–1945, 1991.
27. **Ray R, Snyder RC, Thomas S, Koller CA, Miller DM.** Mithramycin blocks protein binding and function of the SV40 early promoter. *J Clin Invest* 83: 2003–2007, 1989.
28. **Saito H, Yamamoto M, Inui K, Hori R.** Transcellular transport of organic cation across monolayers of kidney epithelial cell line LLC-PK_1. *Am J Physiol Cell Physiol* 262: C59–C66, 1992.
29. **Shimakura J, Terada T, Katsura T, Inui K.** Characterization of the human peptide transporter PEPT1 promoter: Sp1 functions as a basal transcriptional regulator of human PEPT1. *Am J Physiol Gastrointest Liver Physiol* 289: G471–G477, 2005.
30. **Shimakura J, Terada T, Shimada Y, Katsura T, Inui K.** The transcription factor Cdx2 regulates the intestine-specific expression of human peptide transporter 1 through functional interaction with Sp1. *Biochem Pharmacol* 71: 1581–1588, 2006.
31. **Shu Y, Brown C, Castro RA, Shi RJ, Lin ET, Owen RP, Sheardown SA, Yue L, Burchard EG, Brett CM, Giacomini KM.** Effect of genetic variation in the organic cation transporter 1, OCT1, on metformin pharmacokinetics. *Clin Pharmacol Ther.* In press.
32. **Shu Y, Sheardown SA, Brown C, Owen RP, Zhang S, Castro RA, Ianculescu AG, Yue L, Lo JC, Burchard EG, Brett CM, Giacomini KM.** Effect of genetic variation in the organic cation transporter 1 (OCT1) on metformin action. *J Clin Invest* 117: 1422–1431, 2007.
33. **Tanihara Y, Masuda S, Sato T, Katsura T, Ogawa O, Inui K.** Substrate specificity of MATE1 and MATE2-K, human multidrug and toxin extrusions/H^+-organic cation antiporters. *Biochem Pharmacol* 74: 359–371, 2007.
34. **Terada T, Masuda S, Asaka J, Tsuda M, Katsura T, Inui K.** Molecular cloning, functional characterization and tissue distribution of rat H^+/organic cation antiporter MATE1. *Pharm Res* 23: 1696–1701, 2006.
35. **Tsuda M, Terada T, Asaka J, Ueba M, Katsura T, Inui K.** Oppositely directed H^+ gradient functions as a driving force of rat H^+/organic cation antiporter MATE1. *Am J Physiol Renal Physiol* 292: F593–F598, 2007.
36. **Wright SH.** Role of organic cation transporters in the renal handling of therapeutic agents and xenobiotics. *Toxicol Appl Pharmacol* 204: 309–319, 2005.
37. **Zhang X, Cherrington NJ, Wright SH.** Molecular identification and functional characterization of rabbit MATE1 and MATE2-K. *Am J Physiol Renal Physiol* 293: F360–F370, 2007.

Pharmaceutical Research (© 2007)
DOI: 10.1007/s11095-007-9495-x

Research Paper

Thyroid Hormone Regulates the Expression and Function of P-glycoprotein in Caco-2 Cells

Naoki Nishio,[1] Toshiya Katsura,[1] and Ken-ichi Inui[1,2]

Received November 6, 2006; accepted January 26, 2007

Purpose. In patients with thyroid disorders, abnormalities in the pharmacokinetics of various drugs including digoxin, a substrate of P-glycoprotein (Pgp) which plays a crucial role in drug absorption and disposition, have been reported. In this study, we examined the effect of 3,5,3′-L-triiodothyronine (T_3) on the function and expression of Pgp using the human intestinal epithelial cell line Caco-2.

Materials and Methods. The effect of T_3 on the expression of Pgp and MDR1 mRNA was assessed by Western blotting and competitive polymerase chain reaction, respectively. Digoxin uptake and transport by Pgp was assessed using Caco-2 cell monolayers.

Results. The expression of MDR1 mRNA was increased by T_3 treatment in a concentration-dependent manner. Pgp expression was also increased by 100 nM T_3, whereas it decreased on depletion of T_3. The amount of [^{3}H]digoxin accumulated in Caco-2 cell monolayers treated with T_3 was diminished significantly compared with that in control cells. In addition, the basal-to-apical transcellular transport of [^{3}H]digoxin was accelerated by T_3 treatment.

Conclusions. These results indicate that T_3 regulates the expression and function of Pgp. It is possible that changes in Pgp expression alter the pharmacokinetics of Pgp substrates in patients with thyroid disorders.

KEY WORDS: Caco-2 cells; digoxin; P-glycoprotein; 3,5,3′-L-triiodothyronine.

INTRODUCTION

P-glycoprotein (Pgp), a 170 kDa membrane glycoprotein and gene product of MDR1, acts as an ATP-dependent multidrug efflux pump which transports a wide range of hydrophobic compounds such as β-blockers, calcium channel antagonists, anticancer agents, and immunosupressants. Expression of Pgp in humans and rodents is observed in various tissues including the brain, liver, kidney, and small intestine. Therefore, Pgp is considered to be closely related to the absorption, distribution, and excretion of drugs, suggesting that the alteration of Pgp expression levels may affect the pharmacokinetics of drugs (1). Greiner *et al.* (2) showed that the AUC of digoxin, a Pgp substrate, was decreased following an up-regulation of Pgp expression caused by the coadministration of rifampin. Dexamethasone also modulates Pgp expression and affects the pharmacokinetics of Rhodamine 123 in rats (3,4). Pharmacokinetic variations due to changes in Pgp expression levels may be closely related to the efficacy and side effects of drugs.

Thyroid hormone is secreted from the thyroid gland to maintain normal growth, development, body temperature, and energy levels. Most of its effects appear to be mediated by the activation of nuclear receptors that regulate mRNA transcription and subsequent protein synthesis. A change in the serum thyroid hormone level may be followed by the altered expression of proteins that have important physiological functions. In a hyperthyroid state, in addition to an increase in appetite and a reduction in body weight, the pharmacokinetics of drugs such as propranolol (5) and digoxin (6–9) changed dramatically. We previously demonstrated that thyroid hormone induced Pgp and mdr1a/1b mRNA expression in hyperthyroid rats (10). Furthermore, Siegmund *et al.* (11) showed that the administration of levothyroxine tended to up-regulate the expression of MDR1 mRNA and Pgp in healthy volunteers. However, it did not result in major alterations to the pharmacokinetics of talinolol. Therefore, the mechanism of the changes in pharmacokinetics of drugs caused by thyroid hormone remains to be elucidated.

In the present study, to evaluate in further detail the effect of thyroid hormone in the small intestine, we investigated the effect of thyroid hormone on the expression of MDR1 mRNA and Pgp abundance and Pgp function using the human intestinal epithelial cell line Caco-2.

MATERIALS AND METHODS

Materials. [^{3}H]Digoxin (1.37 TBq/mmol) was obtained from PerkinElmer Life and Analytical Sciences (Boston, MA). [^{14}C] Inulin (259 MBq/mmol) was from Moravek Biochemicals Inc.

[1] Department of Pharmacy, Kyoto University Hospital, Faculty of Medicine, Kyoto University, Sakyo-ku, Kyoto, 606-8507, Japan.
[2] To whom correspondence should be addressed. (e-mail: inui@kuhp.kyoto-u.ac.jp)

ABBREVIATIONS: PCR, polymerase chain reaction; Pgp, P-glycoprotein; T_3, 3,5,3′-L-triiodothyronine.